HHS Public Access

Author manuscript

ACS Nano. Author manuscript; available in PMC 2018 September 10.

Published in final edited form as:

ACS Nano. 2018 July 24; 12(7): 6360–6377. doi:10.1021/acsnano.8b02491.

Assessing and Mitigating the Hazard Potential of Two-Dimensional Materials

Linda M. Guiney[†], **Xiang Wang**[ζ], **Tian Xia**[ζ], **André E. Nel**[ζ], and **Mark C. Hersam**[†,‡,&,*]

[†]Department of Materials Science and Engineering, Northwestern University, Evanston, Illinois 60208, USA.

[‡]Department of Chemistry, Northwestern University, Evanston, Illinois 60208, USA.

[&]Department of Medicine, Northwestern University, Evanston, Illinois 60208, USA.

[ζ]Division of NanoMedicine, Department of Medicine; California NanoSystems Institute, University of California, Los Angeles, CA 90095, USA.

Abstract

The family of two-dimensional (2D) materials is comprised of a continually expanding palette of unique compositions and properties with potential applications in electronics, optoelectronics, energy capture and storage, catalysis, and nanomedicine. To accelerate the implementation of 2D materials in widely disseminated technologies, human health and environmental implications need to be addressed. While extensive research has focused on assessing the toxicity and environmental fate of graphene and related carbon nanomaterials, the potential hazards of other 2D materials have only recently begun to be explored. Herein, the toxicity and environmental fate of post-carbon 2D materials, such as transition metal dichalcogenides, hexagonal boron nitride, and black phosphorus, are reviewed as a function of their preparation methods and surface functionalization. Specifically, we delineate how the hazard potential of 2D materials is directly related to structural parameters and physicochemical properties, and how experimental design is critical to the accurate elucidation of the underlying toxicological mechanisms. Finally, a multidisciplinary approach for streamlining the hazard assessment of emerging 2D materials is outlined, thereby providing a pathway for accelerating their safe use in a range of technologically relevant contexts.

Table of Contents Graphic

[*]**Corresponding Author:** Mark C. Hersam, m-hersam@northwestern.edu, Departments of Materials Science and Engineering, Chemistry, and Medicine, Northwestern University, Evanston, Illinois 60208, USA. .

Author Contributions

The manuscript was written through contributions of all authors. All authors have given approval to the final version of the manuscript.

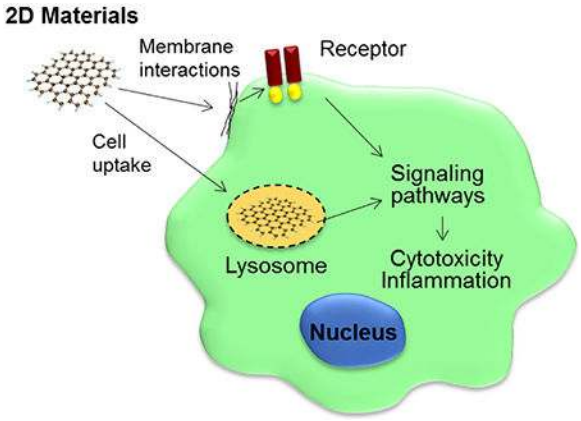

Keywords

transition metal dichalcogenide; hexagonal boron nitride; black phosphorus; toxicity; environmental fate; 2D material; risk assessment; nanotoxicology; safety

Two-dimensional (2D) materials have attracted widespread attention in the research community due to the unique physicochemical properties that emerge in the atomically thin limit, an interest first sparked by the isolation of graphene in 2004.[1–3] The 2D material family encompasses a broad range of mechanical, electrical, thermal, optical, and chemical properties that have been explored for electronic, optoelectronic, energy, and biomedical applications. However, before these promising laboratory-scale prototypes can be widely disseminated in commercialized technologies, the biological and environmental hazards of 2D materials need to be understood and mitigated. While the hazard assessment of graphene and related carbon nanomaterials have been reviewed extensively elsewhere,[4–10] here we focus on post-carbon 2D materials, such as transition metal dichalcogenides (TMDCs), hexagonal boron nitride (hBN), and black phosphorus (BP), that present a broader range of compositions, chemistries, and physicochemical properties, and thus a wider range of potential toxic responses and environmental impacts.

TMDCs are a class of 2D materials that gained significant interest in the wake of graphene due to their broadly tunable electronic band structures, which enable significant opportunities in electronic and optoelectronic applications.[11–13] Like most 2D materials, the properties of TMDCs depend on thickness, particularly in the atomically thin limit.[11,12,14–16] In the bulk, TMDCs are layered materials with a stoichiometry of MX_2, where M represents a group IV, V, or VI transition metal and X represents a chalcogen such as sulfur, selenium, or tellurium.[12] The relatively strong intralayer bonding is covalent, whereas the interlayer interactions are dictated by van der Waals forces. This weak interlayer bonding allows for relatively straightforward exfoliation of the bulk material into few-layer or monolayer form.[17] Thus far, the most widely studied TMDC is molybdenum disulfide (MoS_2). MoS_2 undergoes a transition in its electronic structure from an indirect band gap in the bulk to a direct band gap in the monolayer limit, which gives rise to qualitatively different optical properties such as photoluminescence.[18–21] The semiconducting nature of MoS_2 suggests significant potential in electronic applications, while the optical properties

make it useful for optoelectronic as well as biomedical applications. Beyond semiconductors like MoS_2, the electronic properties of TMDCs also include metallic (*e.g.*, NdS_2) and semimetallic (*e.g.*, WTe_2) behavior.[12]

The library of TMDCs has enabled the development of a wide range of applications, specifically in the biomedical field. Due to their high surface area and chemical reactivity, these materials can be functionalized and used as drug delivery carriers.[22,23] The high surface to volume ratio also makes TMDCs highly sensitive to adsorbed molecules, enabling applications in sensing.[24–30] The intrinsic photoluminescence of some TMDCs further allows their use as biomedical imaging agents. [31–34] Other applications also make use of the optical properties of TMDCs, such as the strong absorption of light and high photothermal conversion efficiencies in a wide range of TMDCs including MoS_2, tungsten disulfide (WS_2), titanium disulfide (TiS_2), rhenium disulfide (ReS_2), and molybdenum diselenide ($MoSe_2$), enabling their use for photothermal therapies.[35–46]

Hexagonal boron nitride (hBN) is another popular layered material that has been explored extensively in recent years, especially in its 2D form.[47] Similar to graphene, the boron and nitrogen atoms are arranged in a hexagonal 2D lattice, resulting in a material with exceptionally high chemical and thermal stability. With a wide band gap of approximately 6 eV, hBN is an electrically insulating material, although it possesses relatively high thermal conductivity.[48–50] With this unique combination of properties, hBN can also be used as a component of electronic systems, concurrently acting as a thermal management material[51–53] and a dielectric.[50,54,55] In the context of biological applications, hBN has gained interest due to its lower cytotoxicity compared to its carbon analogues.[56–60] The high biocompatibility of hBN has resulted in a recent surge of studies exploring biomedical technologies based on this material, including drug delivery, fluorescent labeling in cells, and tissue engineering.[61–67]

Post-carbon elemental 2D materials are also attracting significant interest due to their chemical simplicity and unique properties. Most elemental 2D materials need to be synthesized using highly controlled bottom-up approaches because they do not occur naturally as layered materials in their bulk form.[68] Black phosphorus (BP) is a notable exception, in that the bulk form is layered and relatively stable compared to other allotropes of phosphorus.[69] As a semiconducting, anisotropic 2D material with a layer-dependent band structure, BP has been extensively studied for its use in electronics, optoelectronics, and biomedical applications.[70–77] Although BP is among the most stable forms of phosphorus, it possesses relatively high chemical reactivity compared to other 2D materials such as high environmental instability under ambient conditions and chemical degradation in the presence of oxygen and water.[78–83] While this environmental instability presents challenges for the electronic and optoelectronic applications of BP, chemical degradation pathways present potential opportunities in the biomedical field to create a biodegradable 2D nanomaterial construct. Consequently, research exploring the use of BP for biological imaging, sensing, and therapeutics has accelerated significantly in the last two years,[84–93] motivating the need for systematic exploration of the hazard potential for emerging elemental 2D materials.

Herein, we review the studies to date that have addressed the toxicity of 2D materials, particularly emphasizing the preparation methods and resulting physicochemical properties that dictate their interactions with biological systems. In addition, due to its importance in determining exposure risk, this review summarizes key results from the literature concerning the environmental fate of 2D materials. A thorough understanding of these issues will inform ongoing efforts to realize the design of safer 2D materials.

2D Material Synthesis Methods that Impact Hazard Potential

The physicochemical properties of 2D materials are a direct result of synthesis and processing techniques. A variety of preparation methods exist for monolayer or few-layer 2D materials, which can generally be separated into either bottom-up or top-down approaches.[94] Bottom-up approaches involve the use of atomic or molecular precursors to grow the 2D material. For example, chemical vapor deposition (CVD) of MoS_2 requires solid precursors of molybdenum, usually in the form of molybdenum trioxide (MoO3), and sulfur that are vaporized by heating and subsequently deposited onto a substrate to form thin films of MoS_2.[95–97] Solution-phase synthesis methods such as hydrothermal synthesis[98] or combining precursors such as molybdic acid and thiourea at high temperature and pressure[99] can also be used to prepare TMDCs such as MoS_2. These solution-based methods produce highly polydisperse samples, both in terms of lateral dimensions and number of layers.

Top-down approaches involve the isolation of 2D materials from bulk layered crystals. The most well-known of these approaches is micromechanical cleavage, more commonly referred to as the Scotch tape method.[1,21,100,101] However, due to the low yield of micromechanical cleavage, significant research effort has been devoted to liquid phase exfoliation methods because they are more scalable and enable easier post-processing in manufacturing settings.[102–105] Liquid phase exfoliation methods often use small ionic species, such as lithium, to intercalated between the layers in the bulk material, ultimately facilitating exfoliation.[20,106,107] In particular, the addition of water reacts with intercalated lithium ions, liberating hydrogen gas that weakens the interlayer van der Waals forces, resulting in exfoliation into 2D sheets. For the case of MoS_2, while this process produces monolayer sheets in solution with high yield, the aggressive chemical conditions drive MoS_2 to undergo a phase transformation from trigonal prismatic (2H-MoS_2) to octahedral (1TMoS_2). Since 1T-MoS_2 is a metastable metallic material, it can be partially converted back to 2HMoS_2 through thermal annealing or laser-assisted phase reversion,[14,20,108] although the final structure and properties differ from pristine exfoliated 2H-MoS_2.

Another top-down liquid phase method that has been studied extensively utilizes ultrasonication or shear mixing to exfoliate 2D materials.[104,109–116] To achieve optimal exfoliation yields, the liquid needs to contain a surface energy that is well-matched to the targeted 2D material or additional additives, such as surfactants or stabilizing polymers, need to be added to the solution. While this method is amenable to scale-up and generally yields chemically pristine 2D materials, the resulting flakes are generally small in lateral dimensions and possesses high polydispersity, with the majority of the flakes being few-layer instead of monolayer.[104] Despite these drawbacks, top-down approaches are being most commonly pursued in early-stage industrial efforts due to the low costs involved.[94]

Additionally, post-processing methods such as density gradient ultracentrifugation can be used to sort and isolate monodisperse populations of the 2D materials following liquid phase exfoliation.[54,103,112] In addition, some top-down approaches can be carried out in aqueous media, which eliminates the need for environmentally unfriendly organic solvents.[109,117–122] Consequently, aqueous and biocompatible synthesis and processing have become increasingly important for the application of 2D materials in biomedical contexts.

2D Material Hazard Assessment

The safety of 2D materials is an emerging topic that assesses the potential adverse interactions of these materials at the nano-bio interface. In this section, we highlight several of these initial studies and discuss how their conclusions can inform the design and implementation of improved toxicity screening methods in the future. Specifically, we have categorized the most important characteristics for the hazard assessment of 2D materials including composition, lateral size and thickness, surface functionalization, and crystal structure (Figure 1).

Composition

Chemical composition is one of the most important considerations for determining the biological interactions and fate of 2D materials *in vivo*. The surface chemistry and the dissolution of the material will be determined by its chemical composition, which will in turn affect the cellular interactions, uptake, and biodistribution.[123,124] For 2D materials, several studies have assessed the cytotoxicity of TMDCs according to composition.[125–128] For example, Teo *et al.* investigated the toxicity of chemically exfoliated MoS_2, WS_2, and WSe_2 in human lung carcinoma epithelial cells (A549).[125] While low toxicity of MoS_2 and WS_2 was observed, a dose-dependent toxicity of WSe_2 was detected, indicating that the presence of selenium plays an important role in the toxicity of TMDCs. However, it is unclear whether this toxicity can be attributed to the nano-bio interface interactions caused by the presence of selenium at the surface of the TMDC or the toxicity related to dissolved selenium. A similar study by the same group was recently published on the cytotoxicity of vanadium ditelluride (VTe_2), niobium ditelluride ($NbTe_2$), and tantalum ditelluride ($TaTe_2$) in the same cell line (A549), allowing for direct comparison to the cytotoxicity of MoS_2, WS_2, and WSe_2 from the previous study.[127] High cytotoxicity was observed after exposure to VTe_2, whereas $NbTe_2$ and $TaTe_2$ showed reduced cytotoxicity. Overall, the ditellurides exhibited higher cytotoxicity than the disulfide materials, while WSe_2 exhibited similar cytotoxicity to the ditellurides. To further investigate the role of the chalcogen, the same group ran an identical study comparing the cytotoxicity of vanadium dichalcogenides: VS_2, VSe_2, and VTe_2.[126] VS_2 showed the least cytotoxic effect, whereas VSe_2 and VTe_2 showed similarly higher cytotoxicity, further suggesting that the chalcogen significantly affects the toxicological response.

From these initial studies comparing the cytotoxicity of varying TMDCs, it is clear that the identity of the chalcogen atom plays an important role in the overall cytotoxicity. This observation is most likely due to the differences in chemical reactivity of different chalcogenides, where the more reactive TMDCs result in the release of the chalcogen atoms,

resulting in higher toxicity. These cytotoxicity results as well as those discussed in the following sections are summarized in Table 1. Due to their relatively infrequent study thus far in the field of toxicology, cytotoxicity has been the most widely used metric for gauging the biocompatibility of emerging 2D materials. This empirically reported cytotoxicity provides some insight, but a deeper mechanistic understanding is required to fully assess the hazard potential.

Exfoliation

As layered materials are exfoliated, the fundamental properties of the material change.[17,75] Similarly, biological interactions with layered materials vary as a function of exfoliation state. For example, Chng *et al.* investigated the effects of exfoliation on the cytotoxicity of MoS_2.[129] Using three different lithium sources—methyllithium, n-butyllithium, and tert-butyllithium—MoS_2 was chemically exfoliated, and the exfoliation yield was deduced using Raman spectroscopy. Higher exfoliation yield was achieved with tert-butyllithium and n-butyllithium, which corresponded to higher cytotoxicity. Based on this observation, the study concluded that the increase in surface area and active edge sites leads to higher toxicity in more highly exfoliated MoS_2. However, limited material characterization left open the possibility that other physical properties of these MoS_2 samples led to the differential cytotoxicity. A more thorough investigation of the toxicity of MoS_2 by Wang *et al.* compared two forms of exfoliated MoS_2 to an aggregated form of MoS_2 (Figure 2).[130] The exfoliated forms of MoS_2 were prepared by chemical exfoliation with nbutyllithium and ultrasonication-assisted liquid phase exfoliation with the aid of the surfactant Pluronic F87. The toxicity of these materials was examined *in vitro* and in the mouse lung *in vivo*. Aggregated MoS_2 induced significantly increased production of pro-inflammatory cytokines, indicating a pro-inflammatory response *in vitro*, whereas the lithiated and Pluronic-dispersed MoS_2 showed reduced effects, which was attributed to the bioavailability and cellular uptake of these MoS_2 materials. *In vivo* studies revealed focal areas of inflammation in the lung after acute exposure to aggregated MoS_2 but no significant inflammatory response was observed for any of the MoS_2 materials following sub-chronic exposure. Overall, effective exfoliation reduced the toxic response of MoS_2 compared to its aggregated state, suggesting that stable dispersions of exfoliated MoS_2 lead to higher biocompatibility. Negligible toxicity of exfoliated MoS_2 was also observed by Shah *et al.* in rat pheochromocytoma cells and adrenal medulla endothelial cells.[131] In this work, the MoS_2 materials were also chemically exfoliated, further supporting this synthetic pathway to biocompatible MoS_2.

The cytotoxicity of MoS_2 by different exfoliation and preparation methods has also been explored in a series of recent studies. For instance, a comparative study of the cytotoxicity and genotoxicity in epithelial kidney cells was performed for mechanically exfoliated MoS_2 *versus* MoS_2 that was grown by chemical vapor deposition (CVD).[132] Similar to exfoliated MoS_2 prepared by solution processing methods, both mechanically exfoliated MoS_2 and CVD-grown MoS_2 showed minimal impact on cell morphology in addition to non-significant reactive oxygen species (ROS) generation and negligible effects on cell viability. Furthermore, exfoliated MoS_2 did not induce measurable genetic changes. Similar results for CVD-grown MoS_2 were observed in both mouse embryo fibroblasts (NIH-3T3) and human

adipose-derived mesenchymal stem cells (HAMSCs).[133] In particular, no significant loss of cell viability was observed for MoS_2 concentrations up to 50 μg mL^{-1} and 300 μg mL^{-1} in NIH-3T3 and HAMSCs, respectively. While most studies have found a high degree of biocompatibility for MoS_2, a recent study by Liu *et al.* indicated that exposure to MoS_2 induces a loss in cell viability in HepG2 cells at concentrations as low as 30 μg mL^{-1}.[134] In this case, MoS_2 induced a significant increase in intracellular ROS at doses greater than 2 μg mL^{-1} in addition to membrane damage at doses greater than 4 μg mL^{-1}. The study also found similar results for hBN. Thus, the observed toxicity was attributed to membrane damage caused by the 2D sheet-like structure of the materials. However, the study lacks proper material characterization to rule out other mechanistic possibilities. Overall, the cytotoxicity results for exfoliated MoS_2 have been highly contradictory, resulting from inconsistent material preparation methods, inadequate material characterization, and varying cytotoxicity assays in a wide range of different biological systems as illustrated in Table 1.

For the case of black phosphorus, a study by Latiff *et al.* investigated the cytotoxicity of bulk BP crystals in human lung carcinoma epithelial cells (A549), which showed a dose-dependent toxicity and reduced cell viability at BP concentrations of 50 μg mL^{-1}.[135] In contrast, a later study by Mu *et al.* investigated the toxicity of BP quantum dots (BPQDs) both *in vitro* in HeLa cells and *in vivo* in mice.[136] At high BPQD concentrations of 200 μg mL^{-1}, significant cytotoxicity and apoptotic effects were observed, which were attributed to oxidative stress. Weight loss in the mice after exposure indicated acute toxicity, but the mice eventually recovered, indicating that BPQDs did not induce long-term inflammatory responses or injury. Thus, the exfoliation of BP may play a role in the toxicological response, but additional studies are needed to gain mechanistic insight.

Lateral Size and Thickness

The biological response to a 2D geometry is unique, and the physical interactions of 2D materials with cells are expected to vary based on their aspect ratio and mechanical properties.[137] Thus, the characterization of lateral size and thickness of 2D materials is critical in order to quantify the aspect ratio and its effects on the biological response. Towards this end, Moore *et al.* investigated the role of lateral size of MoS_2 flakes in the cytotoxicity, cellular uptake, and inflammatory response.[138] Using liquid cascade centrifugation, MoS_2 flakes dispersed with sodium cholate of varying lateral sizes were isolated. The response of three separate MoS_2 samples with mean lateral sizes of 50 nm, 117 nm, and 177 nm were studied in A549, AGS, and THP-1 cell lines, chosen specifically to assess risk *via* different exposure routes. At 1 μg mL^{-1} dose, all samples showed minimal cytotoxicity and invariant cell morphology, although an inflammatory response was observed. Assays revealed a size-dependent increase in cytokine production (IL-6, IL-10, IL-13, TNF-α, and IL-1β) in THP-1 cells, with the smallest MoS_2 flake sizes inducing the largest increases in cytokine production. However, the MoS_2 samples were prepared under conditions that suffered from endotoxin contamination, making it difficult to determine if the size-dependent toxicity resulted from the material itself or the increased surface area allowing for increased endotoxin levels. In this case, it is most likely the increase in effective surface area of the 2D material that results in higher endotoxin adsorption and subsequently higher production of inflammatory cytokines. Thus, as the material becomes thinner and

smaller, the available surface area increases, resulting in higher cytotoxicity. To elucidate the fundamental effects of 2D material lateral size on the biological response, the material processing needs to be performed in a manner where other variables, such as endotoxin contamination, are held constant.

More recently, BP has also been used as a model 2D material to probe the effects of lateral size on the cytotoxic response.[139,140] Fu *et al.* prepared BP nanosheets by liquid phase exfoliation and then isolated three different lateral size distributions through varying centrifugation speeds.[139] In human hepatocyte cells (LO2), a small dose-dependent loss of viability was observed, but even at concentrations of 50 μg mL^{-1}, cell viability still exceeded 80%. In a more mechanistic study, three different sizes of BP were prepared by aqueous liquid phase exfoliation and fractional centrifugation (Figure 3).[140] The three samples varied in both lateral size and thickness with BP-1 containing flakes of the largest lateral size and thickness and BP-3 containing flakes of the smallest lateral size and thickness. The cytotoxicity was tested in three cell lines: mouse fibroblasts (NIH-3T3), human colonic epithelial cells, and human embryonic kidney cells (293T). The cytotoxic response was found to be dependent on concentration, size, and cell type, with the 293T cells being the most sensitive and the epithelial cells being the least sensitive. Unlike MoS_2, BP flakes with the largest lateral size and thickness showed the highest levels of cytotoxicity. However, it should be noted that the smallest BP sample in this study was similar in size to the largest MoS_2 sample in the previous study, while the largest BP sample is an order of magnitude larger. Thus, it is likely that at these different length scales, different mechanisms of toxicity will dominate. Additional assays showed ROS generation, but the response was not size-dependent. Further investigation into the interaction of BP with model cell membranes using a quartz crystal microbalance with dissipation monitoring revealed that the largest BP samples disrupted the integrity of the cell membrane, implicating this pathway as the most likely size-dependent toxicity mechanism. Consequently, it appears that the BP flakes induce physical damage to the cell membrane, an interaction that is more extreme with larger sized flakes, resulting in higher cytotoxicity of the larger BP flakes compared to smaller flakes. However, the study did not account for the environmental instability of exfoliated BP, and no stability or long-term (> 24 hours) cytotoxicity data were presented.

Overall, it is clear that the lateral size and thickness of 2D materials affect the overall biological response. The aspect ratio and resulting mechanical properties will also influence cellular interactions and thus biological outcomes, but additionally the lateral size and thickness will determine their biodistribution in tissues. Furthermore, at varying size scales of the 2D materials, different mechanisms of toxicity will play a more dominant role. Thus far, there are no comprehensive studies focusing on the size effects of the biodistribution of 2D materials, and therefore further *in vivo* investigations of this nature are needed in the future.

Structural Forms

Most toxicity studies to date have focused on dispersions of 2D materials because many biological applications, such as drug delivery and imaging agents, call for such a format.[72,141–145] However, 2D materials are also being explored in a myriad of other applications in

which the qualitatively different physical form factors are needed including thin films, three-dimensional constructs, and composites.[146–151] In these cases, biological interactions will fundamentally differ from those of a well-dispersed 2D material in solution. Consequently, some recent studies have begun to specifically probe the toxicity of 2D materials in solid-state formats such as thin films, foams, and composites. One such study investigated the toxicity of MoS_2, WS_2, and hBN coated glass slides, seeding adipose-derived human mesenchymal stem cells (hMSCs) onto these thin films and then studying the cellular response (Figure 4).[152] None of the 2D materials resulted in a significant loss in cell viability up to concentrations of 5 μg mL^{-1}, but rather the cells showed higher cellular adhesion and enhanced proliferation compared to an uncoated glass slide. Furthermore, the presence of the 2D materials contributed to enhanced adipogenesis in the hMSCs.

The biocompatibility of thin films generated from printed 2D material inks was explored by McManus *et al.*[153] In this study, a range of 2D materials, including graphene, MoS_2, WS_2, and hBN, were exfoliated in water in the presence of pyrene sulfonic acid derivatives. To achieve printable viscosities of the exfoliated dispersions, Triton X-100 and propylene glycol were added to the solutions following exfoliation. Cytotoxicity of the 2D inks was then determined using an LDH assay in human lung epithelial cells (A549) and human keratinocyte cells (HaCaT). No loss of cell viability was observed for any of the materials up to concentrations of 100 μg mL^{-1}. Furthermore, cells seeded onto the 2D material thin films showed strong interactions with the substrates, similar to what was observed in the previous study by Suhito *et al.*[152] This favorable cell attachment and high biocompatibility have prompted further studies on the biological interactions of nanostructured films of 2D materials with different cell types, such as differentiation of stem cells.[154] Similar biocompatibility has also been reported for a number of polymer composites containing 2D materials.[64,155–157] Like 2D material thin films, these composites have shown high cell adhesion, low cytotoxicity, and accelerated cell proliferation and growth. While studies exploring these varying structural forms of 2D materials have been limited thus far, it is important to note that by changing the form of the nanomaterial from a dispersion to a thin film or 3D dimensional network, the interface with the biological system fundamentally changes, resulting in different biological outcomes.

Surface Functionalization

Extensive studies on graphene and related carbon nanomaterials have shown that surface functionalization plays a major role in the toxicological response.[158–161] Analogous studies on the surface functionalization of post-carbon 2D materials have begun to be undertaken with an eye toward achieving specific biological outcomes and minimizing toxic response.[162–165] For example, Qu *et al.* showed that functionalization of BPQDs with a titanium sulfonate ligand (TiL_4) resulted in lower cytotoxicity and reduced inflammatory response (Figure 5).[164] In this study, the cytotoxicity of bare BPQDs was compared to that of TiL_4-modified BPQDs in two different macrophage cell lines. Both BPQD samples showed minimal effect on the viability of RAW264.7 macrophage cells. On the other hand, in J774A.1 macrophage cells, bare BPQDs showed a significant loss of viability, while this effect was reduced in the case of TiL_4-modified BPQDs. The proinflammatory response of the BPQDs was also tested by measuring the cytokine (TNF-α) production in RAW264.7

cells. TiL_4-modified BPQDs showed reduced inflammatory response compared to bare BPQDs, which correlated with the cellular uptake of the materials, namely that the intracellular level of bare BPQDs was significantly higher than that of TiL_4-modified BPQDs. Further *in vivo* studies revealed that bare BPQDs showed an acute inflammatory response at 24 hour post-exposure, as evidenced by the significant increase of neutrophils in the blood and concentration of cytokines (TNF-α, eotaxin, IL-6, MCP-1, KC, MIP-1, MIG, VEGF) in the mice serum, whereas TiL_4-modified BPQDs did not show this response. Although neither material demonstrated chronic inflammation, the differences in acute toxicity confirmed that surface functionalization of BP can be used to minimize toxicity by altering cellular uptake. Surface functionalization techniques can also be used to minimize toxicity by changing the degradation behavior of the 2D material. For example, chemically exfoliated MoS_2 functionalized with 2-iodoacetamide showed a higher resistance to enzymatic degradation than non-functionalized chemically exfoliated MoS_2.[165] Upon exposure to the degradation products of both MoS_2 samples, both HeLa and RAW264.7 cells showed a higher loss of viability upon exposure to the degradation products of non-functionalized MoS_2, thus providing evidence that the degradation products at elevated concentrations can induce a toxic response. More generally, the surface functionalization of 2D materials will dictate the dispersion stability, the surface reactivity, and the degradation behavior, all of which will contribute to the overall toxicity of the material.

Environmental Stability and Chemical Dissolution

Although most TMDCs are considered highly stable, some studies have shown that these materials undergo environmental transformations. In particular, the dissolution of TMDCs has been shown to vary as a function of composition due to differences in the strength and reactivity of the bonds formed between metal and chalcogen atoms. By varying the metal atom but otherwise maintaining analogous TMDC structure and processing, Hao *et al.* investigated the *in vitro* cytotoxicity and *in vivo* biodistribution and toxicity of MoS_2, WS_2, and TiS_2 nanosheets (Figure 6).[166] The nanosheets were prepared using a high-temperature solution-phase synthesis method in which bulk TMDCs were ultrasonicated in *N*-methyl-2-pyrrolidone (NMP) and then redispersed in water with the aid of lipoic acid-conjugated polyethylene glycol (PEG). An MTT viability protocol revealed no cytotoxicity up to 200 μg mL^{-1}, and further assays showed no damage to the cell membrane and no increase in ROS for this set of materials. *In vivo* biodistribution after intravenous injection into mice showed accumulation of the TMDCs mainly in the liver and spleen after 1 day, indicating that the TMDCs were most likely taken up by Kupffer cells and spleen macrophages. Despite these apparent similarities among the TMDC samples, other responses varied as a function of the metal atom such as MoS_2 showing the fastest metabolic rate and excretion from the mice, with significant amounts of Mo detected in the urine and feces. *In vitro* degradation of the TMDCs was further used to characterize biodistribution and metabolism. When stored in PBS, WS_2 showed the highest stability, due to the strong W-S covalent bond, while MoS_2 degraded into soluble Mo in the form of MoO_4^{2-}. TiS_2 also oxidized, which resulted in an insoluble precipitate of TiO_2. These differences in chemical reactivity also explain the *in vivo* excretion behavior where MoS_2 is most easily cleared from the system as it degrades to soluble MoO_4^{2-}, whereas WS_2 and TiO_2 persist and accumulate in organs. In a separate study, vanadium disulfide (VS_2) nanosheets showed a similar excretion profile to MoS_2,

accumulating mainly in the liver and spleen of mice, but then degrading into a soluble vanadium oxide species that was easily cleared from the body and detected in the urine and feces.[167]

A study by Song *et al.* found a similar dissolution and biodistribution of molybdenum oxide (MoO_x) nanosheets, but further investigated the role of pH on the dissolution characteristics.[168] In this study, MoO_x nanosheets functionalized with PEG were prepared by a one-pot hydrothermal method and investigated for their capabilities as a photothermal therapeutic agent. The resulting MoO_x nanosheets, while stable in acidic pH, degrade quickly at physiological pH. This pH-dependent degradation was exploited to efficiently accumulate the MoO_x nanosheets in relatively acidic tumor cells, whereas MoO_x nanosheets elsewhere in unaffected cells were excreted quickly and efficiently to avoid long-term retention. Similar to studies on MoS_2, the MoO_x nanosheets accumulated mainly in the liver and spleen but were eventually cleared due to dissolution into soluble molybdate anions. Thus, in the case of environmentally unstable 2D materials, the degradation products need to be identified and their behavior and fate in the biological system need to be well understood in order to accurately assess the hazard of these materials and design schemes to mitigate any potential risks.

Furthermore, the risk associated with 2D materials will be highly dependent on their transport and transformation in the environment. For example, Lanphere *et al.* investigated the transport of two different MoS_2 dispersions in aquatic environments, in which chemically exfoliated MoS_2 was compared to a sample of MoS_2 exfoliated by ultrasonication in the presence of Pluronic F87 as a surfactant.[169] While the Pluronic-dispersed MoS_2 demonstrated high dispersion stability in aqueous solution, the material was more likely to bind irreversibly to the quartz porous media than the chemically exfoliated MoS_2, which was highly mobile in the sand columns. In a more recent study, Zou *et al.* explored the environmental transformation of MoS_2 after exposure to humic acid in an aqueous environment.[170] The chemical dissolution of MoS_2 increased significantly upon exposure to humic acid, and the resulting humic acid-MoS_2 complex showed higher peroxidase-like catalytic activity. In order to better assess their ecological and biological risks, further study is required to understand the environmental transformations of 2D materials, which will in turn affect their biological interactions and outcomes.

Crystal Structure

In addition to the composition, the crystal structure of the material can also play a role in dissolution and biological fate. For example, MoS_2 has two common polytypes: trigonal prismatic (2H) and octahedral (1T). Naturally occurring bulk MoS_2 has a 2H structure, which is maintained following ultrasonication-based exfoliation in solution.[120] However, lithiation-based chemical exfoliation of MoS_2 results in a phase change of the material to 1T.[20] The chemical dissolution pathways of these two polytypes of MoS_2 in biological and environmental media was investigated by Wang *et al.* (Figure 7).[171] 1T-MoS_2 (or ce-MoS_2) was prepared by chemical exfoliation using n-butyllithium, whereas 2H-MoS_2 (or ue-MoS_2) was prepared using ultrasonication in an aqueous solution containing sodium cholate. Rapid oxidation and degradation of the ce-MoS_2 was observed, while the ue-MoS_2 showed a

significantly lower rate of degradation. This preferential degradation of ce-MoS_2 indicates that ce-MoS_2 samples will contain a mixture of soluble ions (*e.g.*, MoO_4^{2-}) and nanosheets during exposure and cellular uptake. This could impact the biological interactions and final biodistribution of the material. In the same study, chemically exfoliated $MoSe_2$ was also investigated and showed a similar oxidative dissolution to ce-MoS_2. However, unlike ce-MoS_2, the chalcogen product in this case will be insoluble, having different implications for its biological interactions and fate. Additionally, the bulk form of MoS_2 did not show significant dissolution, indicating that the dissolution of MoS_2 is accelerated as its thickness approaches the 2D limit.

The environmental stability of 2D materials has clear implications for toxicity and fate, and thus needs to be considered when assessing hazard potential. Additionally, a greater understanding of the material properties and environmental factors that influence stability and dissolution of 2D materials provides opportunities for engineering biomedical constructs with desirable degradation properties. This concept of designing biodegradable 2D materials for biomedical applications has grown in recent years due to the ambient instability of black phosphorus in the presence of water and oxygen.[85,90,172] While many BP constructs have been proposed for biological imaging, drug delivery, sensing, and theranostics, limited research has been devoted to the understanding the degradation of BP and the resulting byproducts, which will be imperative to safely utilizing this 2D material in biomedical contexts. With the emergence of other environmentally unstable 2D materials such as indium selenide (InSe), the field of biodegradable 2D materials is likely to expand in the future.[173]

Future Outlook

The growing interest in the use of 2D materials in electronics, optoelectronics, energy capture and storage, and biomedical applications necessitates the need to understand their health and environmental implications. The interactions of nanomaterials with a biological system are dictated by the physicochemical properties of the material.[174–179] In this review, we presented several important factors that play a role at the nano-bio interface including composition, exfoliation method, flake size and thickness, surface functionalization, crystal structure, and chemical dissolution. More comprehensive material characterization is necessary to integrate ongoing toxicity studies of 2D materials into a meaningful hazard assessment. Similarly, since the synthesis and processing protocols significantly affect the resulting structure and properties of 2D material, these details should always be included in toxicological reports. Finally, a detailed understanding of how 2D material structure and properties and behavior change in biological media is critical for determining hazard potential in biomedical contexts. Specifically, the dispersion stability, particle size, and dissolution rate can vary significantly in biologically relevant media due to changes in pH and the presence of salts and proteins, which have the potential to fundamentally alter how 2D materials interact with or are taken up by cells.[180]

In addition to thorough material characterization, thoughtful design of toxicity studies is required for 2D materials. When investigating *in vitro* cytotoxicity of these materials, the cell line selection will play a large role in the measured toxicological response, especially since certain cell lines have already shown different sensitivities to 2D material exposure.

[140,164] Thus, it is important to resist the temptation to generalize cytotoxicity results for different cell lines based on any single study. To date, cytotoxicity of emerging 2D materials has focused mainly on biomedical exposure due to the obvious implications for biomedical technologies.[137,181,182] However, because 2D materials are being explored for a wide range of applications and industries, occupational and environmental exposure also merit investigation. Understanding the effects of all potential exposure routes will provide the most comprehensive picture of the hazard potential associated with 2D materials.

The lack of thorough material characterization, consistent design of *in vitro* assays, and mechanistic understanding of the cytotoxic response has led to contradictory reports of the biocompatibility of many 2D materials. Additionally, the cytotoxicity of the 2D materials in most cases is reported as a simple quantification of cell viability, without details of the characterization of cell growth or cell morphology that would enable better comparison across studies. To provide a more comprehensive understanding of the toxicity mechanisms of 2D materials, we thus recommend an interdisciplinary approach that relates the physicochemical properties of the materials to specific biological endpoints (Figure 8). Nanomaterial libraries should also be used to systematically vary the physicochemical properties of the 2D material of interest. Ideally, thoroughly characterized and monodisperse populations of 2D materials should be used to isolate the effects of specific characteristics (*e.g.*, lateral size, thickness, surface functionalization, and electronic structure) on biological outcomes. Using *in vitro* high throughput screening (HTS) assays, cellular interactions can be elucidated by quantifying the biodistribution, inflammation, fibrosis, and metabolic functions as a result of exposure to 2D materials. These results can then be validated by limited, carefully designed *in vivo* assays. In addition to the acute exposure testing, the long-term biodistribution and effects need to be investigated. From the initial toxicity studies of TMDCs, it is clear that some of these materials persist in organs and tissues, and thus bioaccumulation of 2D materials may present long-term repercussions.[166]

The field of 2D material research is still accelerating, with continual discovery of additional 2D materials and phenomena associated with their unique structures and compositions.[173,183,184] With a constantly expanding library of 2D materials, the ability to predict toxicological outcomes is of critical importance. Recent 2D materials of interest, such as black phosphorus, indium selenide, and germanium sulfide, demonstrate high environmental instability.[185–187] In these cases, a firm understanding of the dissolution behavior in addition to the temporal evolution of material properties is paramount for both their biomedical application as well as understanding the health and environmental risks of these materials. While some studies have begun to probe the toxicological effects of structural parameters such as lateral size, thickness, and surface functionalization, the effects of the electronic structure of 2D materials remain largely unexplored. In the case of MoS_2, it has been observed that the crystal structure and resulting change in electronic properties results in a change in the dissolution behavior of the material,[171] thus motivating further studies along these lines.[188] Overall, a comprehensive assessment of the hazard potential of 2D materials requires an interdisciplinary approach to elucidate the relationship between the physicochemical properties of the materials and the resulting biological outcomes. In this manner, predictive toxicological models can be developed that will ultimately enable the

development of mitigation schemes that will accelerate the safe use of 2D materials in widely used technological applications.

ACKNOWLEDGMENTS

This work was supported by the National Science Foundation and the Environmental Protection Agency under Award No. DBI-1266377. The authors also acknowledge support from the National Institute of Environmental Health Sciences of the National Institutes of Health under Award Number RO1ES022698. The content is solely the responsibility of the authors and does not necessarily represent the official views of the sponsors.

VOCABULARY

Two-dimensional material
Planar material that is generally layered in structure with relatively weak interlayer bonding that allows for facile exfoliation down to the monolayer limit

Liquid phase exfoliation
Solution-based process in which energy is added to the system through sonication or shear mixing to exfoliate two-dimensional materials

Cytotoxicity
Injury or death of a cell

Cytokine
Small proteins or biomolecules secreted by the cell in the immune response

Reactive oxygen species
Oxygen-containing molecules or materials that are reactive in nature and can result in cellular damage at high levels

Biodistribution
Movement and fate of materials within a biological system

REFERENCES

(1). Novoselov K; Geim A; Morozov S Electric Field Effect in Atomically Thin Carbon Films. Science 2004, 306, 666–669. [PubMed: 15499015]

(2). Geim AK; Novoselov KS The Rise of Graphene. Nat. Mater 2007, 6, 183–191. [PubMed: 17330084]

(3). Geim AK Graphene: Status and Prospects. Science 2009, 324, 1530–1535. [PubMed: 19541989]

(4). Sanchez VC; Jachak A; Hurt RH; Kane AB Biological Interactions of Graphene-Family Nanomaterials–An Interdisciplinary Review. Chem. Res. Toxicol 2012, 25, 15–34. [PubMed: 21954945]

(5). Zhao J; Wang Z; White JC; Xing B Graphene in the Aquatic Environment: Adsorption, Dispersion, Toxicity and Transformation. Environ. Sci. Technol 2014, 48, 9995–10009. [PubMed: 25122195]

(6). Volkov Y; McIntyre J; Prina-Mello A Graphene Toxicity as a Double-Edged Sword of Risks and Exploitable Opportunities: A Critical Analysis of the Most Recent Trends and Developments. 2D Mater. 2017, 4, 22001.

(7). Gurunathan S; Kim JH Synthesis, Toxicity, Biocompatibility, and Biomedical Applications of Graphene and Graphene-Related Materials. Int. J. Nanomedicine 2016, 11, 1927–1945. [PubMed: 27226713]

(8). Pattnaik S; Swain K; Lin Z Graphene and Graphene-Based Nanocomposites: Biomedical Applications and Biosafety. J. Mater. Chem. B 2016, 4, 7813–7831.

(9). Zhang Q; Wu Z; Li N; Pu Y; Wang B; Zhang T; Tao J Advanced Review of Graphene-Based Nanomaterials in Drug Delivery Systems: Synthesis, Modification, Toxicity and Application. Mater. Sci. Eng. C 2017, 77, 1363–1375.

(10). Chng ELK; Pumera M Toxicity of Graphene Related Materials and Transition Metal Dichalcogenides. RSC Adv. 2015, 5, 3074–3080.

(11). Chhowalla M; Shin HS; Eda G; Li L-J; Loh KP; Zhang H The Chemistry of Two-Dimensional Layered Transition Metal Dichalcogenide Nanosheets. Nat. Chem 2013, 5, 263–275. [PubMed: 23511414]

(12). Wang QH; Kalantar-Zadeh K; Kis A; Coleman JN; Strano MS Electronics and Optoelectronics of Two-Dimensional Transition Metal Dichalcogenides. Nat. Nanotechnol 2012, 7, 699–712. [PubMed: 23132225]

(13). Manzeli S; Ovchinnikov D; Pasquier D; Yazyev OV; Kis A 2D Transition Metal Dichalcogenides. Nat. Rev. Mater 2017, 2, 17033.

(14). Lv R; Robinson JA; Schaak RE; Sun D; Sun Y; Mallouk TE; Terrones M Transition Metal Dichalcogenides and Beyond: Synthesis, Properties, and Applications of Single- and Few-Layer Nanosheets. Acc. Chem. Res 2015, 48, 56–64. [PubMed: 25490673]

(15). Sorkin V; Pan H; Shi H; Quek SY; Zhang YW Nanoscale Transition Metal Dichalcogenides: Structures, Properties, and Applications. Crit. Rev. Solid State Mater. Sci 2014, 39, 319–367.

(16). Koski KJ; Cui Y The New Skinny in Two-Dimensional Nanomaterials. ACS Nano 2013, 7, 3739–3743. [PubMed: 23678956]

(17). Butler S; Hollen S; Cao L; Cui Y Progress, Challenges, and Opportunities in Two-Dimensional Materials Beyond Graphene. ACS Nano 2013, 7, 2898–2926. [PubMed: 23464873]

(18). Eknapakul T; King PDC; Asakawa M; Buaphet P; Takagi H; Shen KM; Baumberger F; Sasagawa T; Jungthawan S; Meevasana W Electronic Structure of a Quasi-Freestanding MoS_2 Monolayer. Nano Lett. 2014, 14, 1312–1316. [PubMed: 24552197]

(19). Kuc A; Zibouche N; Heine T Influence of Quantum Confinement on the Electronic Structure of the Transition Metal Sulfide TS_2. Phys. Rev. B 2011, 83, 245213.

(20). Eda G; Yamaguchi H; Voiry D; Fujita T; Chen M; Chhowalla M Photoluminescence from Chemically Exfoliated MoS_2. Nano Lett 2011, 11, 5111–5116. [PubMed: 22035145]

(21). Splendiani A; Sun L; Zhang Y; Li T; Kim J; Chim C-Y; Galli G; Wang F Emerging Photoluminescence in Monolayer MoS_2. Nano Lett. 2010, 10, 1271–1275. [PubMed: 20229981]

(22). Yin W; Yan L; Yu J; Tian G; Zhou L; Zheng X; Zhang X; Yong Y; Li J; Gu Z; Zhao Y High-Throughput Synthesis of Single-Layer MoS_2 Nanosheets as a Near-Infrared Photothermal-Triggered Drug Delivery for Effective Cancer Therapy. ACS Nano 2014, 8, 6922–6933. [PubMed: 24905027]

(23). Li BL; Setyawati MI; Chen L; Xie J; Ariga K; Lim CT; Garaj S; Leong DT Directing Assembly and Disassembly of 2D MoS_2 Nanosheets with DNA for Drug Delivery. ACS Appl. Mater. Interfaces 2017, 9, 15286–15296. [PubMed: 28452468]

(24). Pumera M; Loo AH Layered Transition-Metal Dichalcogenides (MoS_2 and WS_2) for Sensing and Biosensing. TrAC Trends Anal. Chem 2014, 61, 49–53.

(25). Lee J; Dak P; Lee Y; Park H; Choi W; Alam MA; Kim S Two-Dimensional Layered MoS_2 Biosensors Enable Highly Sensitive Detection of Biomolecules. Sci. Rep 2014, 4, 7352. [PubMed: 25516382]

(26). Wang L; Wang Y; Wong JI; Palacios T; Kong J; Yang HY Functionalized MoS_2 Nanosheet-Based Field-Effect Biosensor for Label-Free Sensitive Detection of Cancer Marker Proteins in Solution. Small 2014, 10, 1101–1105. [PubMed: 24474708]

(27). Sarkar D; Liu W; Xie X; Anselmo A MoS_2 Field-Effect Transistor for Next-Generation Label-Free Biosensors. ACS Nano 2014, 8, 3992–4003. [PubMed: 24588742]

(28). Gan X; Zhao H; Quan X Two-Dimensional MoS_2: A Promising Building Block for Biosensors. Biosens. Bioelectron 2017, 89, 56–71. [PubMed: 27037158]

(29). Li Z; Wong SL Functionalization of 2D Transition Metal Dichalcogenides for Biomedical Applications. Mater. Sci. Eng. C 2016, 70, 1095–1106.

(30). Mo L; Li J; Liu Q; Qiu L; Tan W Nucleic Acid-Functionalized Transition Metal Nanosheets for Biosensing Applications. Biosens. Bioelectron 2017, 89, 201–211. [PubMed: 27020066]

(31). Ou JZ; Chrimes AF; Wang Y; Tang S; Strano MS; Kalantar-zadeh K Ion-Driven Photoluminescence Modulation of Quasi-Two-Dimensional MoS_2 Nanoflakes for Applications in Biological Systems. Nano Lett. 2014, 14, 857–863. [PubMed: 24397241]

(32). Kong R-M; Ding L; Wang Z; You J; Qu F A Novel Aptamer-Functionalized MoS_2 Nanosheet Fluorescent Biosensor for Sensitive Detection of Prostate Specific Antigen. Anal. Bioanal. Chem 2015, 407, 369–377. [PubMed: 25366976]

(33). Wang N; Wei F; Qi Y; Li H; Lu X Synthesis of Strongly Fluorescent Molybdenum Disulfide Nanosheets for Cell-Targeted Labeling. ACS Appl. Mater. Interfaces 2014, 6, 19888–19894. [PubMed: 25380411]

(34). Bai X; Wang J; Mu X; Yang J; Liu H; Xu F; Jing Y; Liu L; Xue X; Dai H; Liu Q; Sun Y-M; Liu C; Zhang X-D Ultrasmall WS_2 Quantum Dots with Visible Fluorescence for Protection of Cells and Animal Models from Radiation-Induced Damages. ACS Biomater. Sci. Eng 2017, 3, 460–470.

(35). Chen L; Feng Y; Zhou X; Zhang Q; Nie W; Wang W; Zhang Y; He C One-Pot Synthesis of MoS_2 Nanoflakes with Desirable Degradability for Photothermal Cancer Therapy. ACS Appl. Mater. Interfaces 2017, 9, 17347–17358. [PubMed: 28471183]

(36). Deng R; Yi H; Fan F; Fu L; Zeng Y; Wang Y; Li Y; Liu Y; Ji S; Su Y Facile Exfoliation of MoS_2 Nanosheets by Protein as a Photothermal-Triggered Drug Delivery System for Synergistic Tumor Therapy. RSC Adv. 2016, 6, 77083–77092.

(37). Liu T; Wang C; Gu X; Gong H; Cheng L; Shi X; Feng L; Sun B; Liu Z Drug Delivery with PEGylated MoS_2 Nano-Sheets for Combined Photothermal and Chemotherapy of Cancer. Adv. Mater 2014, 26, 3433–3440. [PubMed: 24677423]

(38). Cheng L; Liu J; Gu X; Gong H; Shi X; Liu T; Wang C; Wang X; Liu G; Xing H; Bu W; Sun B; Liu Z PEGylated WS_2 Nanosheets as a Multifunctional Theranostic Agent for *In Vivo* Dual-Modal CT/Photoacoustic Imaging Guided Photothermal Therapy. Adv. Mater 2014, 26, 1886–1893. [PubMed: 24375758]

(39). Qian X; Shen S; Liu T; Cheng L; Liu Z Two-Dimensional TiS_2 Nanosheets for *In Vivo* Photoacoustic Imaging and Photothermal Cancer Therapy. Nanoscale 2015, 7, 6380–6387. [PubMed: 25786074]

(40). Ren Q; Li B; Peng Z; He G; Zhang W; Guan G; Huang X; Xiao Z; Liao L; Pan Y; Yang X; Zou R; Hu J SnS Nanosheets for Efficient Photothermal Therapy. New J. Chem 2016, 40, 4464–4467.

(41). Shen S; Chao Y; Dong Z; Wang G; Yi X; Song G; Yang K; Liu Z; Cheng L Bottom-Up Preparation of Uniform Ultrathin Rhenium Disulfide Nanosheets for Image-Guided Photothermal Radiotherapy. Adv. Funct. Mater 2017, 27, 1700250.

(42). Liu T; Chao Y; Gao M; Liang C; Chen Q; Song G; Cheng L; Liu Z Ultra-Small MoS2 Nanodots with Rapid Body Clearance for Photothermal Cancer Therapy. Nano Res. 2016, 9, 3003–3017.

(43). Li Z; Shao J; Luo Q; Yu XF; Xie H; Fu H; Tang S; Wang H; Han G; Chu PK Cell-Borne 2D Nanomaterials for Efficient Cancer Targeting and Photothermal Therapy. Biomaterials 2017, 133, 37–48. [PubMed: 28426974]

(44). Zhong C; Zhao X; Wang L; Li Y; Zhao Y Facile Synthesis of Biocompatible $MoSe_2$ Nanoparticles for Efficient Targeted Photothermal Therapy of Human Lung Cancer. RSC Adv. 2017, 7, 7382–7391.

(45). Peng MY; Zheng DW; Wang SB; Cheng SX; Zhang XZ Multifunctional Nanosystem for Synergistic Tumor Therapy Delivered by Two-Dimensional MoS_2. ACS Appl. Mater. Interfaces 2017, 9, 13965–13975. [PubMed: 28378999]

(46). Wang S; Zhao J; Yang H; Wu C; Hu F; Chang H; Li G; Ma D; Zou D; Huang M Bottom-up Synthesis of WS_2 Nanosheets with Synchronous Surface Modification for Imaging Guided Tumor Regression. Acta Biomater. 2017, 58, 442–454. [PubMed: 28611005]

(47). Luo W; Wang Y; Hitz E; Lin Y; Yang B; Hu L Solution Processed Boron Nitride Nanosheets: Synthesis, Assemblies and Emerging Applications. Adv. Funct. Mater 2017, 27, 1701450.

(48). Watanabe K; Taniguchi T; Kanda H Direct-Bandgap Properties and Evidence for Ultraviolet Lasing of Hexagonal Boron Nitride Single Crystal. Nat. Mater 2004, 3, 404–409. [PubMed: 15156198]

(49). Golberg D; Bando Y; Huang Y; Terao T; Mitome M; Tang C; Zhi C Boron Nitride Nanotubes and Nanosheets. ACS Nano 2010, 4, 2979–2993. [PubMed: 20462272]

(50). Song L; Ci L; Lu H; Sorokin PB; Jin C; Ni J; Kvashnin AG; Kvashnin DG; Lou J; Yakobson BI; Ajayan PM Large Scale Growth and Characterization of Atomic Hexagonal Boron Nitride Layers. Nano Lett. 2010, 10, 3209–3215. [PubMed: 20698639]

(51). Loeblein M; Tsang SH; Pawlik M; Phua EJR; Yong H; Zhang XW; Gan CL; Teo EHT High-Density 3D-Boron Nitride and 3D-Graphene for High-Performance Nano-Thermal Interface Material. ACS Nano 2017, 11, 2033–2044. [PubMed: 28157329]

(52). Kuang Z; Chen Y; Lu Y; Liu L; Hu S; Wen S; Mao Y; Zhang L Fabrication of Highly Oriented Hexagonal Boron Nitride Nanosheet/Elastomer Nanocomposites with High Thermal Conductivity. Small 2015, 11, 1655–1659. [PubMed: 25365940]

(53). Song WL; Wang P; Cao L; Anderson A; Meziani MJ; Farr AJ; Sun YP Polymer/Boron Nitride Nanocomposite Materials for Superior Thermal Transport Performance. Angew. Chemie - Int. Ed 2012, 51, 6498–6501.

(54). Zhu J; Kang J; Kang J; Jariwala D; Wood JD; Seo JWT; Chen KS; Marks TJ; Hersam MC Solution-Processed Dielectrics Based on Thickness-Sorted Two-Dimensional Hexagonal Boron Nitride Nanosheets. Nano Lett. 2015, 15, 7029–7036. [PubMed: 26348822]

(55). Fang H; Bai SL; Wong CP Thermal, Mechanical and Dielectric Properties of Flexible BN Foam and BN Nanosheets Reinforced Polymer Composites for Electronic Packaging Application. Compos. Part A Appl. Sci. Manuf 2017, 100, 71–80.

(56). Ciofani G; Danti S; Genchi GG; Mazzolai B; Mattoli V Boron Nitride Nanotubes: Biocompatibility and Potential Spill-Over in Nanomedicine. Small 2013, 9, 1672–1685. [PubMed: 23423826]

(57). Ciofani G; Raffa V; Menciassi A; Cuschieri A Cytocompatibility, Interactions, and Uptake of Polyethyleneimine-Coated Boron Nitride Nanotubes by Living Cells: Confirmation of Their Potential for Biomedical Applications. Biotechnol. Bioeng 2008, 101, 850–858. [PubMed: 18512259]

(58). Chen X; Wu P; Rousseas M; Okawa D; Gartner Z; Zettl A; Bertozzi CR Boron Nitride Nanotubes Are Noncytotoxic and Can Be Functionalized for Interaction with Proteins and Cells. J. Am. Chem. Soc 2009, 131, 890–891. [PubMed: 19119844]

(59). Mallineni SSK; Shannahan J; Raghavendra AJ; Rao AM; Brown JM; Podila R Biomolecular Interactions and Biological Responses of Emerging Two-Dimensional Materials and Aromatic Amino Acid Complexes. ACS Appl. Mater. Interfaces 2016, 8, 16604–16611. [PubMed: 27281436]

(60). Atila A; Halici Z; Cadirci E; Karakus E; Palabiyik SS; Ay N; Bakan F; Yilmaz S Study of the Boron Levels in Serum after Implantation of Different Ratios Nano-Hexagonal Boron Nitride-Hydroxy Apatite in Rat Femurs. Mater. Sci. Eng. C 2016, 58, 1082–1089.

(61). Lin L; Xu Y; Zhang S; Ross IM; Ong ACM; Allwood DA Fabrication and Luminescence of Monolayered Boron Nitride Quantum Dots. Small 2014, 10, 60–65. [PubMed: 23839969]

(62). Weng Q; Wang B; Wang X; Hanagata N; Li X; Liu D; Wang X; Jiang X; Bando Y; Golberg D Highly Water-Soluble, Porous, and Biocompatible Boron Nitrides for Anticancer Drug Delivery. ACS Nano 2014, 8, 6123–6130. [PubMed: 24797563]

(63). Rajabi AH; Jaffe M; Arinzeh TL Piezoelectric Materials for Tissue Regeneration: A Review. Acta Biomater. 2015, 24, 12–23. [PubMed: 26162587]

(64). Farshid B; Lalwani G; Shir Mohammadi M; Simonsen J; Sitharaman B Boron Nitride Nanotubes and Nanoplatelets as Reinforcing Agents of Polymeric Matrices for Bone Tissue Engineering. J. Biomed. Mater. Res. - Part B Appl. Biomater 2017, 105, 406–419. [PubMed: 26526153]

(65). Shuai C; Han Z; Feng P; Gao C; Xiao T; Peng S Akermanite Scaffolds Reinforced with Boron Nitride Nanosheets in Bone Tissue Engineering. J. Mater. Sci. Mater. Med 2015, 26, 188. [PubMed: 25917828]

(66). Lu T; Wang L; Jiang Y; liu Q; Huang C Hexagonal Boron Nitride Nanoplates as Emerging Biological Nanovectors and Their Potential Applications in Biomedicine. J. Mater. Chem. B 2016, 4, 6103–6110.

(67). Kumar V; Nikhil K; Roy P; Lahiri D; Lahiri I Emergence of Fluorescence in Boron Nitride Nanoflakes and Its Application in Bioimaging. RSC Adv. 2016, 6, 48025–48032.

(68). Mannix AJ; Kiraly B; Hersam MC; Guisinger NP Synthesis and Chemistry of Elemental 2D Materials. Nat. Rev. Chem 2017, 1, 0014.

(69). Bridgman PW Two New Modifications of Phosphorus. J. Am. Chem. Soc 1914, 36, 1344–1363.

(70). Xia F; Wang H; Jia Y Rediscovering Black Phosphorus as an Anisotropic Layered Material for Optoelectronics and Electronics. Nat. Commun 2014, 5, 4458. [PubMed: 25041752]

(71). Ling X; Wang H; Huang S; Xia F; Dresselhaus MS The Renaissance of Black Phosphorus. Proc. Natl. Acad. Sci 2015, 112, 4523–4530. [PubMed: 25820173]

(72). Qian X; Gu Z; Chen Y Two-Dimensional Black Phosphorus Nanosheets for Theranostic Nanomedicine. Mater. Horiz 2017, 4, 800–816.

(73). Lee HU; Park SY; Lee SC; Choi S; Seo S; Kim H; Won J; Choi K; Kang KS; Park HG; Kim H-S; An HR; Jeong K-H; Lee Y-C; Lee J Black Phosphorus (BP) Nanodots for Potential Biomedical Applications. Small 2016, 12, 214–219. [PubMed: 26584654]

(74). Buscema M; Groenendijk DJ; Blanter SI; Steele GA; Van Der Zant HSJ; Castellanos-Gomez A Fast and Broadband Photoresponse of Few-Layer Black Phosphorus Field-Effect Transistors. Nano Lett. 2014, 14, 3347–3352. [PubMed: 24821381]

(75). Li L; Kim J; Jin C; Ye GJ; Qiu DY; Da Jornada FH; Shi Z; Chen L; Zhang Z; Yang F; Watanabe K; Taniguchi T; Ren W; Louie SG; Chen XH; Zhang Y; Wang F Direct Observation of the Layer-Dependent Electronic Structure in Phosphorene. Nat. Nanotechnol 2017, 12, 21–25. [PubMed: 27643457]

(76). Tran V; Soklaski R; Liang Y; Yang L Layer-Controlled Band Gap and Anisotropic Excitons in Few-Layer Black Phosphorus. Phys. Rev. B 2014, 89, 235319.

(77). Eswaraiah V; Zeng Q; Long Y; Liu Z Black Phosphorus Nanosheets: Synthesis, Characterization and Applications. Small 2016, 12, 3480–3502. [PubMed: 27225670]

(78). Brent JR; Ganguli AK; Kumar V; Lewis DJ; McNaughter PD; O'Brien P; Sabherwal P; Tedstone AA On the Stability of Surfactant-Stabilised Few-Layer Black Phosphorus in Aqueous Media. RSC Adv. 2016, 6, 86955–86958.

(79). Favron A; Gaufrès E; Fossard F; Phaneuf-Laheureux AL; Tang NYW; Lévesque PL; Loiseau A; Leonelli R; Francoeur S; Martel R Photooxidation and Quantum Confinement Effects in Exfoliated Black Phosphorus. Nat. Mater 2015, 14, 826–832. [PubMed: 26006004]

(80). Hu Z; Li Q; Lei B; Zhou Q; Xiang D; Lyu Z; Hu F; Wang J; Ren Y; Guo R; Eda G; Wan L; Han C; Wang J; Chen W Water-Catalyzed Oxidation of Few-Layer Black Phosphorous in a Dark Environment. Angew. Chemie - Int. Ed 2017, 56, 9131–9135.

(81). Zhou Q; Chen Q; Tong Y; Wang J Light-Induced Ambient Degradation of Few-Layer Black Phosphorus: Mechanism and Protection. Angew. Chemie - Int. Ed 2016, 55, 11437–11441.

(82). Abellan G; Wild S; Lloret V; Scheuschner N; Gillen R; Mundloch U; Maultzsch J; Varela M; Hauke F; Hirsch A Fundamental Insights into the Degradation and Stabilization of Thin Layer Black Phosphorus. J. Am. Chem. Soc 2017, 139, 10432–10440. [PubMed: 28675300]

(83). Huang Y; Qiao J; He K; Bliznakov S; Sutter E; Chen X; Luo D; Meng F; Su D; Decker J; Ji W; Ruoff RS; Sutter P Interaction of Black Phosphorus with Oxygen and Water. Chem. Mater 2016, 28, 8330–8339.

(84). Yin F; Hu K; Chen S; Wang D; Zhang J; Xie M; Yang D; Qiu M; Zhang H; Li Z Black Phosphorus Quantum Dot Based Novel SiRNA Delivery Systems in Human Pluripotent Teratoma PA-1 Cells. J. Mater. Chem. B 2017, 5, 5433–5440.

(85). Tao W; Zhu X; Yu X; Zeng X; Xiao Q; Zhang X; Ji X; Wang X; Shi J; Zhang H; Mei L Black Phosphorus Nanosheets as a Robust Delivery Platform for Cancer Theranostics. Adv. Mater 2017, 29, 1603276.

(86). Chen W; Ouyang J; Liu H; Chen M; Zeng K; Sheng J; Liu Z; Han Y; Wang L; Li J; Deng L; Liu Y-N; Guo S Black Phosphorus Nanosheet-Based Drug Delivery System for Synergistic Photodynamic/Photothermal/Chemotherapy of Cancer. Adv. Mater 2017, 29, 1603864.

(87). Chen W; Ouyang J; Yi X; Xu Y; Niu C; Zhang W; Wang L; Sheng J; Deng L; Liu Y-N; Guo S Black Phosphorus Nanosheets as a Neuroprotective Nanomedicine for Neurodegenerative Disorder Therapy. Adv. Mater 2018, 30, 1703458.

(88). Chen Y; Ren R; Pu H; Chang J; Mao S; Chen J Field-Effect Transistor Biosensors with Two-Dimensional Black Phosphorus Nanosheets. Biosens. Bioelectron 2017, 89, 505–510. [PubMed: 27040183]

(89). Gu W; Yan Y; Pei X; Zhang C; Ding C; Xian Y Fluorescent Black Phosphorus Quantum Dots as Label-Free Sensing Probes for Evaluation of Acetylcholinesterase Activity. Sensors Actuators, B Chem. 2017, 250, 601–607.

(90). Shao J; Xie H; Huang H; Li Z; Sun Z; Xu Y; Xiao Q; Yu X-F; Zhao Y; Zhang H; Wang H; Chu PK Biodegradable Black Phosphorus-Based Nanospheres for *In Vivo* Photothermal Cancer Therapy. Nat. Commun 2016, 7, 12967. [PubMed: 27686999]

(91). Zhao Y; Tong L; Li Z; Yang N; Fu H; Wu L; Cui H; Zhou W; Wang J; Wang H; Chu PK; Yu X-F Stable and Multifunctional Dye-Modified Black Phosphorus Nanosheets for Near-Infrared Imaging-Guided Photothermal Therapy. Chem. Mater 2017, 29, 7131–7139.

(92). Guo T; Wu Y; Lin Y; Xu X; Lian H; Huang G; Liu J-Z; Wu X; Yang H-H Black Phosphorus Quantum Dots with Renal Clearance Property for Efficient Photodynamic Therapy. Small 2017, 14, 1702815.

(93). Lv R; Yang D; Yang P; Xu J; He F; Gai S; Li C; Dai Y; Yang G; Lin J Integration of Upconversion Nanoparticles and Ultrathin Black Phosphorus for Efficient Photodynamic Theranostics under 808 nm Near-Infrared Light Irradiation. Chem. Mater 2016, 28, 4724–4734.

(94). Fiori G; Bonaccorso F; Iannaccone G; Palacios T; Neumaier D; Seabaugh A; Banerjee SK; Colombo L Electronics Based on Two-Dimensional Materials. Nat. Nanotechnol 2014, 9, 768–779. [PubMed: 25286272]

(95). Zhan Y; Liu Z; Najmaei S; Ajayan PM; Lou J Large-Area Vapor-Phase Growth and Characterization of MoS_2 Atomic Layers on a SiO_2 Substrate. Small 2012, 8, 966–971. [PubMed: 22334392]

(96). Liu H; Si M; Najmaei S; Neal AT; Du Y; Ajayan PM; Lou J; Ye PD Statistical Study of Deep Sub-Micron Dual-Gated Field-Effect Transistors on Monolayer CVD Molybdenum Disulfide Films. Nano Lett. 2013, 13, 2640–2646. [PubMed: 23679044]

(97). Lee YH; Zhang XQ; Zhang W; Chang MT; Lin C-T; Chang K-D; Yu YC; Wang JT-W; Chang CS; Li L-J; Lin T-W Synthesis of Large-Area MoS_2 Atomic Layers with Chemical Vapor Deposition. Adv. Mater 2012, 24, 2320–2325. [PubMed: 22467187]

(98). Peng Y; Meng Z; Zhong C; Lu J; Yu W Hydrothermal Synthesis of MoS_2 and Its Pressure-Related Crystallization. J. Solid State Chem 2001, 159, 170–173.

(99). Ramakrishna Matte HSS; Gomathi A; Manna AK; Late DJ; Datta R; Pati SK; Rao CNR MoS_2 and WS_2 Analogues of Graphene. Angew. Chemie - Int. Ed 2010, 49, 4059–4062.

(100). Mak KF; Lee C; Hone J; Shan J; Heinz TF Atomically Thin MoS_2: A New Direct-Gap Semiconductor. Phys. Rev. Lett 2010, 105, 136805. [PubMed: 21230799]

(101). Radisavljevic B; Radenovic A; Brivio J; Giacometti V; Kis A Single-Layer MoS_2 Transistors. Nat. Nanotechnol 2011, 6, 147–150. [PubMed: 21278752]

(102). Paton KR; Varrla E; Backes C; Smith RJ; Khan U; O'Neill A; Boland C; Lotya M; Istrate OM; King P; Higgins T; Barwich S; May P; Puczkarski P; Ahmed I; Moebius M; Pettersson H; Long E; Coelho J; O'Brien SE; et al. Scalable Production of Large Quantities of Defect-Free Few-Layer Graphene by Shear Exfoliation in Liquids. Nat. Mater 2014, 13, 624–630. [PubMed: 24747780]

(103). Kang J; Sangwan VK; Wood JD; Hersam MC Solution-Based Processing of Monodisperse Two-Dimensional Nanomaterials. Acc. Chem. Res 2017, 50, 943–951. [PubMed: 28240855]

(104). Coleman J; Lotya M; O'Neill A; Bergin S Two-Dimensional Nanosheets Produced by Liquid Exfoliation of Layered Materials. Science 2011, 331, 568–571. [PubMed: 21292974]

(105). Nicolosi V; Chhowalla M; Kanatzidis MG; Strano MS; Coleman JN Liquid Exfoliation of Layered Materials. Science 2013, 340, 1226419.

(106). Dines MB Lithium Intercalation *via* N-Butyllithium of the Layered Transition Metal Dichalcogenides. Mater. Res. Bull 1975, 10, 287–291.

(107). Joensen P; Frindt RF; Morrison SR Single-Layer MoS_2. Mater. Res. Bull 1986, 21, 457–461.

(108). Fan X; Xu P; Zhou D; Sun Y; Li YC; Nguyen MAT; Terrones M; Mallouk TE Fast and Efficient Preparation of Exfoliated 2H MoS_2 Nanosheets by Sonication-Assisted Lithium Intercalation and Infrared Laser-Induced 1T to 2H Phase Reversion. Nano Lett. 2015, 15, 5956–5960. [PubMed: 26288218]

(109). Smith RJ; King PJ; Lotya M; Wirtz C; Khan U; De S; O'Neill A; Duesberg GS; Grunlan JC; Moriarty G; Chen J; Wang J; Minett AI; Nicolosi V; Coleman JN Large-Scale Exfoliation of Inorganic Layered Compounds in Aqueous Surfactant Solutions. Adv. Mater 2011, 23, 3944–3948. [PubMed: 21796689]

(110). May P; Khan U; Hughes JM; Coleman JN Role of Solubility Parameters in Understanding the Steric Stabilization of Exfoliated Two-Dimensional Nanosheets by Adsorbed Polymers. J. Phys. Chem. C 2012, 116, 11393–11400.

(111). Seo JT; Green AA; Antaris AL; Hersam MC High-Concentration Aqueous Dispersions of Graphene Using Nonionic, Biocompatible Block Copolymers. J. Phys. Chem. Lett 2011, 2, 1004–1008.

(112). Kang J; Seo J-WT; Alducin D; Ponce A; Yacaman MJ; Hersam MC Thickness Sorting of Two-Dimensional Transition Metal Dichalcogenides via Copolymer-Assisted Density Gradient Ultracentrifugation. Nat. Commun 2014, 5, 5478. [PubMed: 25391315]

(113). Halim U; Zheng CR; Chen Y; Lin Z; Jiang S; Cheng R; Huang Y; Duan X A Rational Design of Cosolvent Exfoliation of Layered Materials by Directly Probing Liquid-Solid Interaction. Nat. Commun 2013, 4, 2213. [PubMed: 23896793]

(114). Kang J; Wood JD; Wells SA; Lee JH; Liu X; Chen KS; Hersam MC Solvent Exfoliation of Electronic-Grade, Two-Dimensional Black Phosphorus. ACS Nano 2015, 9, 3596–3604. [PubMed: 25785299]

(115). Varrla E; Backes C; Paton KR; Harvey A; Gholamvand Z; Mccauley J; Coleman JN Large-Scale Production of Size-Controlled MoS_2 Nanosheets by Shear Exfoliation. Chem. Mater 2015, 27, 1129–1139.

(116). Yao Y; Lin Z; Li Z; Song X; Moon K-S; Wong C Large-Scale Production of Two-Dimensional Nanosheets. J. Mater. Chem 2012, 22, 13494–13499.

(117). Guardia L; Paredes JI; Rozada R; Villar-Rodil S; Martínez-Alonso A; Tascón JMD Production of Aqueous Dispersions of Inorganic Graphene Analogues by Exfoliation and Stabilization with Non-Ionic Surfactants. RSC Adv. 2014, 4, 14115–14127.

(118). Kang J; Wells SA; Wood JD; Lee J; Liu X Stable Aqueous Dispersions of Optically and Electronically Active Phosphorene. Proc. Natl. Acad. Sci. U. S. A 2016, 113, 11688–11693. [PubMed: 27092006]

(119). Siepi M; Morales-Narváez E; Domingo N; Monti DM; Notomista E; Merkoçi A Production of Biofunctionalized MoS_2 Flakes with Rationally Modified Lysozyme: A Biocompatible 2D Hybrid Material. 2D Mater. 2017, 4, 035007.

(120). Mansukhani ND; Guiney LM; Kim PJ; Zhao Y; Alducin D; Ponce A; Larios E; Yacaman MJ; Hersam MC High-Concentration Aqueous Dispersions of Nanoscale 2D Materials Using Nonionic, Biocompatible Block Copolymers. Small 2016, 12, 294–300. [PubMed: 26618498]

(121). Ayán-Varela M; Pérez-Vidal Ó; Paredes JI; Munuera JM; Villar-Rodil S; Díaz-González M; Fernández-Sánchez C; Silva VS; Cicuéndez M; Vila M; Martinez-Alonso A; Tascón JMD Aqueous Exfoliation of Transition Metal Dichalcogenides Assisted by DNA/RNA Nucleotides: Catalytically Active and Biocompatible Nanosheets Stabilized by Acid-Base Interactions. ACS Appl. Mater. Interfaces 2017, 9, 2835–2845. [PubMed: 28029778]

(122). Paredes JI; Munuera JM; Villar-Rodil S; Guardia L; Ayán-Varela M; Pagán A; Aznar-Cervantes SD; Cenis JL; Martínez-Alonso A; Tascón JMD Impact of Covalent Functionalization on the Aqueous Processability, Catalytic Activity, and Biocompatibility of Chemically Exfoliated MoS_2 Nanosheets. ACS Appl. Mater. Interfaces 2016, 8, 27974–27986.

(123). Nel A; Xia T; Meng H; Wang X; Lin S; Ji Z; Zhang H Nanomaterial Toxicity Testing in the 21st Century: Use of a Predictive Toxicological Approach and High-Throughput Screening. Acc. Chem. Res 2013, 46, 607–621. [PubMed: 22676423]

(124). Zhu M; Nie G; Meng H; Xia T; Nel A; Zhao Y Physicochemical Properties Determine Nanomaterial Cellular Uptake, Transport, and Fate. Acc. Chem. Res 2013, 46, 622–631. [PubMed: 22891796]

(125). Teo WZ; Chng ELK; Sofer Z; Pumera M Cytotoxicity of Exfoliated Transition-Metal Dichalcogenides (MoS_2, WS_2, and WSe_2) Is Lower than That of Graphene and Its Analogues. Chemistry 2014, 20, 9627–9632. [PubMed: 24976159]

(126). Latiff NM; Sofer Z; Fisher AC; Pumera M Cytotoxicity of Exfoliated Layered Vanadium Dichalcogenides. Chem. - A Eur. J 2017, 23, 684–690.

(127). Chia HL; Latiff NM; Sofer Z; Pumera M Cytotoxicity of Group 5 Transition Metal Ditellurides (MTe2; M=V, Nb, Ta). Chem. - A Eur. J 2018, 24, 206–211.

(128). Shang E; Niu J; Li Y; Zhou Y; Crittenden JC Comparative Toxicity of Cd, Mo, and W Sulphide Nanomaterials toward *E. Coli* under UV Irradiation. Environ. Pollut 2017, 224, 606–614. [PubMed: 28258860]

(129). Chng ELK; Sofer Z; Pumera M MoS_2 Exhibits Stronger Toxicity with Increased Exfoliation. Nanoscale 2014, 6, 14412–14418. [PubMed: 25341082]

(130). Wang X; Mansukhani ND; Guiney LM; Ji Z; Chang CH; Wang M; Liao YP; Song T. Bin; Sun B; Li R; Xia T; Hersam MC; Nel AE Differences in the Toxicological Potential of 2D *versus* Aggregated Molybdenum Disulfide in the Lung. Small 2015, 11, 5079–5087. [PubMed: 26237579]

(131). Shah P; Narayanan TN; Li C-Z; Alwarappan S Probing the Biocompatibility of MoS_2 Nanosheets by Cytotoxicity Assay and Electrical Impedance Spectroscopy. Nanotechnology 2015, 26, 315102. [PubMed: 26183754]

(132). Appel JH; Li DO; Podlevsky JD; Debnath A; Green AA; Wang QH; Chae J Low Cytotoxicity and Genotoxicity of Two-Dimensional MoS_2 and WS_2. ACS Biomater. Sci. Eng 2016, 2, 361–367.

(133). Rashkow JT; Talukdar Y; Lalwani G; Sitharaman B Interactions of 1D- and 2D-Layered Inorganic Nanoparticles with Fibroblasts and Human Mesenchymal Stem Cells. Nanomedicine 2015, 10, 1693–1706. [PubMed: 26080694]

(134). Liu S; Shen Z; Wu B; Yu Y; Hou H; Zhang X-X; Ren H Cytotoxicity and Efflux Pump Inhibition Induced by Molybdenum Disulfide and Boron Nitride Nanomaterials with Sheetlike Structure. Environ. Sci. Technol 2017, 51, 10834–10842. [PubMed: 28841301]

(135). Latiff NM; Teo WZ; Sofer Z; Fisher AC; Pumera M The Cytotoxicity of Layered Black Phosphorus. Chem. - A Eur. J 2015, 21, 13991–13995.

(136). Mu X; Wang J-Y; Bai X; Xu F; Liu H; Yang J; Jing Y; Liu L; Xue X; Dai H; Liu Q; Sun Y-M; Liu C; Zhang X-D Black Phosphorus Quantum Dot Induced Oxidative Stress and Toxicity in Living Cells and Mice. ACS Appl. Mater. Interfaces 2017, 9, 20399–20409. [PubMed: 28553710]

(137). Wang Z; Zhu W; Qiu Y; Yi X; von dem Bussche A; Kane A; Gao H; Koski K; Hurt R Biological and Environmental Interactions of Emerging Two-Dimensional Nanomaterials. Chem. Soc. Rev 2016, 45, 1750–1780. [PubMed: 26923057]

(138). Moore C; Movia D; Smith RJ; Hanlon D; Lebre F; Lavelle EC; Byrne HJ; Coleman JN; Volkov Y; McIntyre J Industrial Grade 2D Molybdenum Disulphide (MoS_2): An *In Vitro* Exploration of the Impact on Cellular Uptake, Cytotoxicity, and Inflammation. 2D Mater. 2017, 4, 025065.

(139). Fu H; Li Z; Xie H; Sun Z; Wang B; Huang H; Han G; Wang H; Chu PK; Yu X-F Different-Sized Black Phosphorus Nanosheets with Good Cytocompatibility and High Photothermal Performance. RSC Adv. 2017, 7, 14618–14624.

(140). Zhang X; Zhang Z; Zhang S; Li D; Ma W; Ma CX; Wu F; Zhao Q; Yan Q; Xing B Size Effect on the Cytotoxicity of Layered Black Phosphorus and Underlying Mechanisms. Small 2017, 13, 1701210.

(141). Kalantar-zadeh K; Ou JZ; Daeneke T; Strano MS; Pumera M; Gras SL Two-Dimensional Transition Metal Dichalcogenides in Biosystems. Adv. Funct. Mater 2015, 25, 5086–5099.

(142). Chimene D; Alge DL; Gaharwar AK Two-Dimensional Nanomaterials for Biomedical Applications: Emerging Trends and Future Prospects. Adv. Mater 2015, 27, 7261–7284. [PubMed: 26459239]

(143). Li Z; Wong SL Functionalization of 2D Transition Metal Dichalcogenides for Biomedical Applications. Mater. Sci. Eng. C 2017, 70, 1095–1106.

(144). Yin F; Gu B; Lin Y; Panwar N; Tjin SC; Qu J; Lau SP; Yong K-T Functionalized 2D Nanomaterials for Gene Delivery Applications. Coord. Chem. Rev 2017, 347, 77–97.

(145). Chen H; Liu T; Su Z; Shang L; Wei G 2D Transition Metal Dichalcogenide Nanosheets for Photo/Thermo-Based Tumor Imaging and Therapy. Nanoscale Horizons 2018, DOI: 10.1039/c7nh00158d.

(146). Finn DJ; Lotya M; Cunningham G; Smith RJ; McCloskey D; Donegan JF; Coleman JN Inkjet Deposition of Liquid-Exfoliated Graphene and MoS_2 Nanosheets for Printed Device Applications. J. Mater. Chem. C 2014, 2, 925–932.

(147). Hossain RF; Deaguero IG; Boland T; Kaul AB Solution Dispersed 2D Graphene & MoS2 for an Inkjet Printed Biocompatible Photodetector. Proc. 25th Bienn. Lester Eastman Conf. High Perform. Devices, LEC 2016, 19–22.

(148). Eksik O; Gao J; Shojaee SA; Thomas A; Chow P; Bartolucci SF; Lucca DA; Koratkar N Epoxy Nanocomposites with Two-Dimensional Transition Metal Dichalcogenide Additives. ACS Nano 2014, 8, 5282–5289. [PubMed: 24754702]

(149). Chan K; Wong H; Yeung K; Tjong S Polypropylene Biocomposites with Boron Nitride and Nanohydroxyapatite Reinforcements. Materials (Basel). 2015, 8, 992–1008. [PubMed: 28787984]

(150). Ternary P; Wan S; Li Y; Peng J; Hu H; Cheng Q; Jiang L Synergistic Toughening of Graphene Oxide-Molybdenum Disulfide-Thermoplastic Polyurethane Ternary Artificial Nacre. ACS Nano 2015, 9, 708–714. [PubMed: 25559751]

(151). Jakus AE; Secor EB; Rutz AL; Jordan SW; Hersam MC; Shah RN Three-Dimensional Printing of High-Content Graphene Scaffolds for Electronic and Biomedical Applications. ACS Nano 2015, 9, 4636–4648. [PubMed: 25858670]

(152). Suhito IR; Han Y; Kim D-S; Son H; Kim T-H Effects of Two-Dimensional Materials on Human Mesenchymal Stem Cell Behaviors. Biochem. Biophys. Res. Commun 2017, 493, 578–584. [PubMed: 28867185]

(153). McManus D; Vranic S; Withers F; Sanchez-Romaguera V; Macucci M; Yang H; Sorrentino R; Parvez K; Son S-K; Iannaccone G; Kostarelos K; Fiori G; Casiraghi C Water-Based and Biocompatible 2D Crystal Inks for All-Inkjet-Printed Heterostructures. Nat. Nanotechnol 2017, 12, 343–350. [PubMed: 28135260]

(154). Wang S; Qiu J; Guo W; Yu X; Nie J; Zhang J; Zhang X; Liu Z; Mou X; Li L; Liu H A Nanostructured Molybdenum Disulfide Film for Promoting Neural Stem Cell Neuronal Differentiation: Toward a Nerve Tissue-Engineered 3D Scaffold. Adv. Biosyst 2017, 1, 1600042.

(155). Jakus AE; Taylor SL; Geisendorfer NR; Dunand DC; Shah RN Metallic Architectures from 3D-Printed Powder-Based Liquid Inks. Adv. Funct. Mater 2015, 25, 6985–6995.

(156). Wang X; Li T; Ma H; Zhai D; Jiang C; Chang J; Wang J; Wu CA 3D-Printed Scaffold with MoS_2 Nanosheets for Tumor Therapy and Tissue Regeneration. NPG Asia Mater. 2017, 9, e376.

(157). Lalwani G; Henslee AM; Farshid B; Lin L; Kasper FK; Qin Y-X; Mikos AG; Sitharaman B Two-Dimensional Nanostructure-Reinforced Biodegradable Polymeric Nanocomposites for Bone Tissue Engineering. Biomacromolecules 2013, 14, 900–909. [PubMed: 23405887]

(158). Guo X; Mei N Assessment of the Toxic Potential of Graphene Family Nanomaterials. J. Food Drug Anal 2014, 22, 105–115. [PubMed: 24673908]

(159). Duch M; Budinger G; Liang Y Minimizing Oxidation and Stable Nanoscale Dispersion Improves the Biocompatibility of Graphene in the Lung. Nano Lett. 2011, 11, 5201–5207. [PubMed: 22023654]

(160). Wang X; Duch MC; Mansukhani N; Ji Z; Liao YP; Wang M; Zhang H; Sun B; Chang CH; Li R; Lin S; Meng H; Xia T; Hersam MC; Nel AE Use of a Pro-Fibrogenic Mechanism-Based Predictive Toxicological Approach for Tiered Testing and Decision Analysis of Carbonaceous Nanomaterials. ACS Nano 2015, 9, 3032–3043. [PubMed: 25646681]

(161). Seabra AB; Paula AJ; de Lima R; Alves OL; Duran N Nanotoxicity of Graphene and Graphene Oxide. Chem. Res. Toxicol 2014, 27, 159–168. [PubMed: 24422439]

(162). Ji D; Zhang Y; Zang Y; Li J; Chen G; He X; Tian H Targeted Intracellular Production of Reactive Oxygen Species by a 2D Molybdenum Disulfide Glycosheet. Adv. Mater 2016, 28, 9356–9363. [PubMed: 27570946]

(163). Dou WT; Kong Y; He XP; Chen GR; Zang Y; Li J; Tian H GPCR Activation and Endocytosis Induced by a 2D Material Agonist. ACS Appl. Mater. Interfaces 2017, 9, 14709–14715. [PubMed: 28401756]

(164). Qu G; Liu W; Zhao Y; Gao J; Xia T; Shi J; Hu L; Zhou W; Gao J; Wang H; Luo Q; Zhou Q; Liu S; Yu X-F; Jiang G Improved Biocompatibility of Black Phosphorus Nanosheets by Chemical Modification. Angew. Chemie - Int. Ed 2017, 56, 14488–14493.

(165). Kurapati R; Muzi L; de Garibay APR; Russier J; Voiry D; Vacchi IA; Chhowalla M; Bianco A Enzymatic Biodegradability of Pristine and Functionalized Transition Metal Dichalcogenide MoS_2 Nanosheets. Adv. Funct. Mater 2017, 27, 1605176.

(166). Hao J; Song G; Liu T; Yi X; Yang K; Cheng L; Liu Z *In Vivo* Long-Term Biodistribution, Excretion, and Toxicology of PEGylated Transition-Metal Dichalcogenides MS_2 (M = Mo, W, Ti) Nanosheets. Adv. Sci 2017, 4, 1600160.

(167). Chen Y; Cheng L; Dong Z; Chao Y; Lei H; Zhao H; Wang J; Liu Z Degradable Vanadium Disulfide Nanostructures with Unique Optical and Magnetic Functions for Cancer Theranostics. Angew. Chemie - Int. Ed 2017, 129, 13171–13176.

(168). Song G; Hao J; Liang C; Liu T; Gao M; Cheng L; Hu J; Liu Z Degradable Molybdenum Oxide Nanosheets with Rapid Clearance and Efficient Tumor Homing Capabilities as a Therapeutic Nanoplatform. Angew. Chemie - Int. Ed 2016, 55, 2122–2126.

(169). Lanphere JD; Luth CJ; Guiney LM; Mansukhani ND; Hersam MC; Walker SL Fate and Transport of Molybdenum Disulfide Nanomaterials in Sand Columns. Environ. Eng. Sci 2015, 32, 163–173. [PubMed: 25741176]

(170). Zou W; Zhou Q; Zhang X; Hu X Environmental Transformations and Algal Toxicity of Single-Layer Molybdenum Disulfide Regulated by Humic Acid. Environ. Sci. Technol 2018, 52, 2638–2648. [PubMed: 29425036]

(171). Wang Z; Von Dem Bussche A; Qiu Y; Valentin TM; Gion K; Kane AB; Hurt RH Chemical Dissolution Pathways of MoS_2 Nanosheets in Biological and Environmental Media. Environ. Sci. Technol 2016, 50, 7208–7217. [PubMed: 27267956]

(172). Fojtů M; Chia X; Sofer Z; Masařík M; Pumera M Black Phosphorus Nanoparticles Potentiate the Anticancer Effect of Oxaliplatin in Ovarian Cancer Cell Line. Adv. Funct. Mater 2017, 27, 1701955.

(173). Boukhvalov D; Gürbulak B; Duman S; Wang L; Politano A; Caputi L; Chiarello G; Cupolillo A The Advent of Indium Selenide: Synthesis, Electronic Properties, Ambient Stability and Applications. Nanomaterials 2017, 7, 372.

(174). Riaz Ahmed KB; Nagy AM; Brown RP; Zhang Q; Malghan SG; Goering PL Silver Nanoparticles: Significance of Physicochemical Properties and Assay Interference on the Interpretation of *In Vitro* Cytotoxicity Studies. Toxicol. Vitr 2017, 38, 179–192.

(175). Albanese A; Tang PS; Chan WCW The Effect of Nanoparticle Size, Shape, and Surface Chemistry on Biological Systems. Annu. Rev. Biomed. Eng 2012, 14, 1–16. [PubMed: 22524388]

(176). Sayes CM; Warheit DB Characterization of Nanomaterials for Toxicity Assessment. Wiley Interdiscip. Rev. Nanomedicine Nanobiotechnology 2009, 1, 660–670. [PubMed: 20049823]

(177). Carnovale C; Bryant G; Shukla R; Bansal V Size, Shape and Surface Chemistry of Nano-Gold Dictate Its Cellular Interactions, Uptake and Toxicity. Prog. Mater. Sci 2016, 83, 152–190.

(178). Oomen AG; Steinhäuser KG; Bleeker EAJ; van Broekhuizen F; Sips A; Dekkers S; Wijnhoven SWP; Sayre PG Risk Assessment Frameworks for Nanomaterials: Scope, Link to Regulations, Applicability, and Outline for Future Directions in View of Needed Increase in Efficiency. NanoImpact 2018, 9.

(179). Nel AE; Mädler L; Velegol D; Xia T; Hoek EMV; Somasundaran P; Klaessig F; Castranova V; Thompson M Understanding Biophysicochemical Interactions at the Nano–Bio Interface. Nat. Mater 2009, 8, 543–557. [PubMed: 19525947]

(180). Mudunkotuwa IA; Grassian VH Biological and Environmental Media Control Oxide Nanoparticle Surface Composition: The Roles of Biological Components (Proteins and Amino Acids), Inorganic Oxyanions and Humic Acid. Environ. Sci. Nano 2015, 2, 429–439.

(181). Kenry; Lim CT Biocompatibility and Nanotoxicity of Layered Two-Dimensional Nanomaterials. ChemNanoMat 2017, 3, 5–16.

(182). Fojtů M; Teo WZ; Pumera M Environmental Impact and Potential Health Risks of 2D Nanomaterials. Environ. Sci. Nano 2017, 4, 1617–1633.

(183). Tan C; Lai Z; Zhang H Ultrathin Two-Dimensional Multinary Layered Metal Chalcogenide Nanomaterials. Adv. Mater 2017, 29, 1701392.

(184). Huang S; Ling X Black Phosphorus: Optical Characterization, Properties and Applications. Small 2017, 13, 1700823.

(185). Ye Y; Guo Q; Liu X; Liu C; Wang J; Liu Y; Qiu J Two-Dimensional GeSe as an Isostructural and Isoelectronic Analogue of Phosphorene: Sonication-Assisted Synthesis, Chemical Stability, and Optical Properties. Chem. Mater 2017, 29, 8361–8368.

(186). Li Z; Qiao H; Guo Z; Ren X; Huang Z; Qi X; Dhanabalan SC; Ponraj JS; Zhang D; Li J; Zhao J; Zhong J; Zhang H High-Performance Photo-Electrochemical Photodetector Based on Liquid-Exfoliated Few-Layered InSe Nanosheets with Enhanced Stability. Adv. Funct. Mater 2017, 1705237.

(187). Island JO; Steele GA; Van Der Zant HSJ; Castellanos-Gomez A Environmental Instability of Few-Layer Black Phosphorus. 2D Mater. 2015, 2, 011002.

(188). Zhang H; Ji Z; Xia T; Meng H; Low-Kam C; Liu R; Pokhrel S; Lin S; Wang X; Liao Y-P; Wang M; Li L; Rallo R; Damoiseaux R; Telesca D; Mädler L; Cohen Y; Zink JI; Nel AE Use of Metal Oxide Nanoparticle Band Gap To Develop a Predictive Paradigm for Oxidative Stress and Acute Pulmonary Inflammation. ACS Nano 2012, 6, 4349–4368. [PubMed: 22502734]

(189). Green AA; Hersam MC Solution Phase Production of Graphene with Controlled Thickness *via* Density Differentiation. Nano Lett. 2009, 9, 4031–4036. [PubMed: 19780528]

(190). Ryder CR; Wood JD; Wells SA; Hersam MC Chemically Tailoring Semiconducting Two-Dimensional Transition Metal Dichalcogenides and Black Phosphorus. ACS Nano 2016, 10, 3900–3917. [PubMed: 27018800]

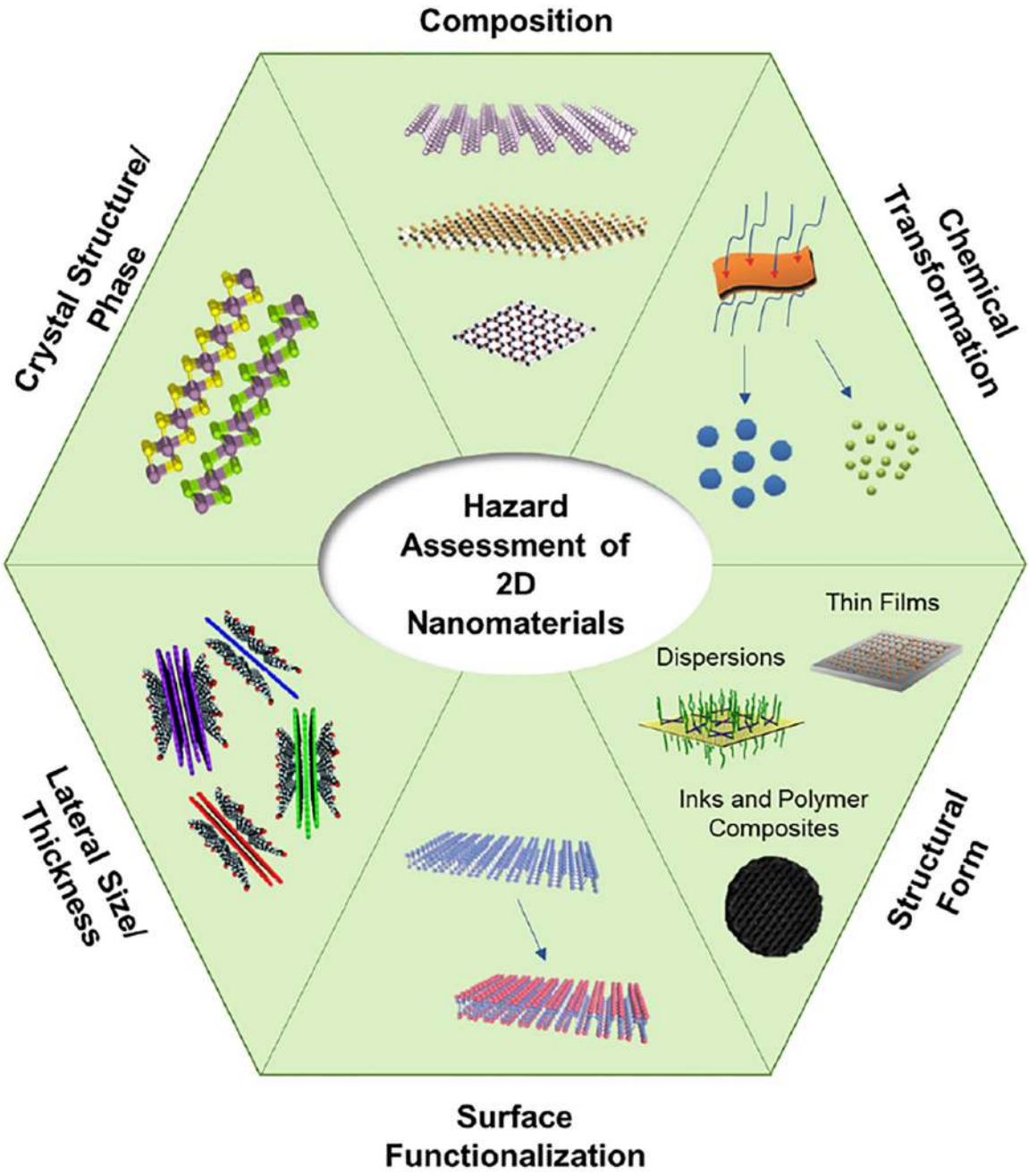

Figure 1.

Physicochemical properties and related factors for 2D materials that affect their toxicity. Complete characterization of these properties is needed to accurately assess the hazard potential for each 2D material. Figure adapted from references[103,120,130,152,156,164,166,189,190]

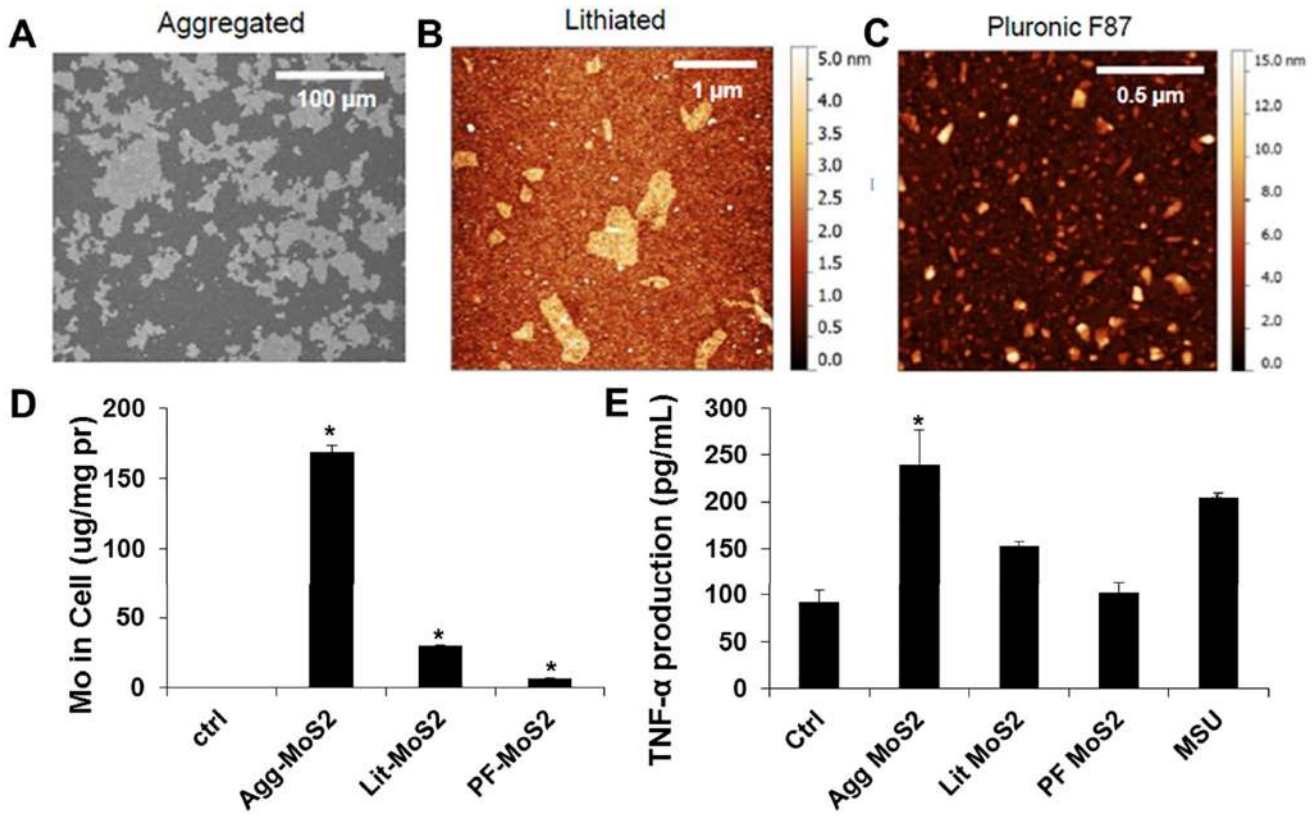

Figure 2.

Effects of aqueous exfoliation methods on the pulmonary hazard potential of molybdenum disulfide (MoS_2). (A) Scanning electron micrograph of aggregated MoS_2. (B) Atomic force microscopy (AFM) image of chemically exfoliated MoS_2 using a lithiation process. (C) AFM image of MoS_2 exfoliated by ultrasonication in the presence of Pluronic F87. The representative AFM images show the differences in lateral size and thickness of the MoS_2 materials as a function of exfoliation method. (D) Cellular content of molybdenum (Mo) and (E) TNF-α production in THP-1 cells 24 hours after exposure to 50 μg mL^{-1} of the MoS_2 samples. The cellular association and uptake correlates well with the proinflammatory effects observed for the MoS_2 materials, indicating that bioavailability plays a key role in the production of cytokines and chemokines. Figure adapted from reference[130]

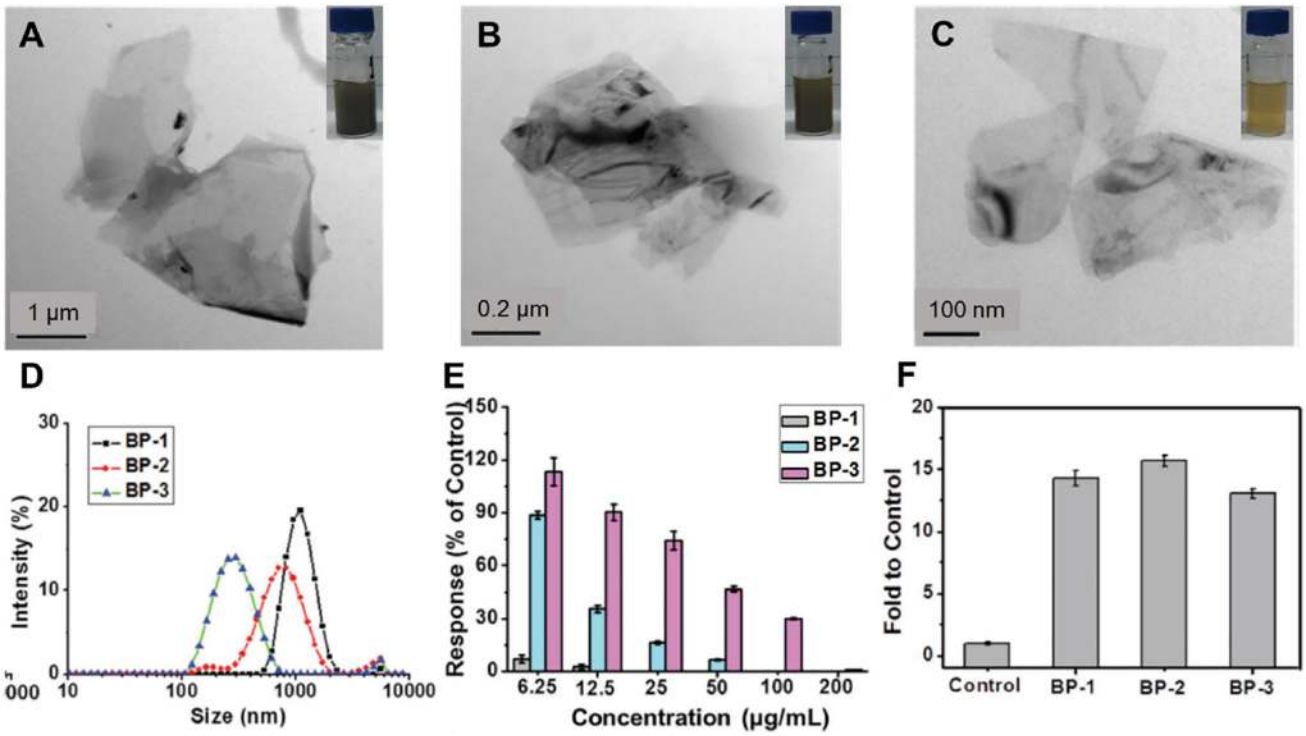

Figure 3.

Effects of lateral size and thickness on the hazard potential of exfoliated black phosphorus (BP). Representative transmission electron micrographs of flakes from three different sized BP dispersions, namely, BP-1 (A), BP-2 (B) and BP-3 (C), and the corresponding photographs of the dispersions (insets). (D) Size measurements of the three BP dispersions in 10% FBS supplemented cell culture medium as determined by dynamic light scattering. (E) Cell viability of NIH-3T3 cells after 24 hours exposure to the BP samples. (F) Intracellular detection of reactive oxygen species in NIH-3T3 cells after exposure to 10 μg mL^{-1} of the BP samples for 4 hours. Figure adapted from reference[140]

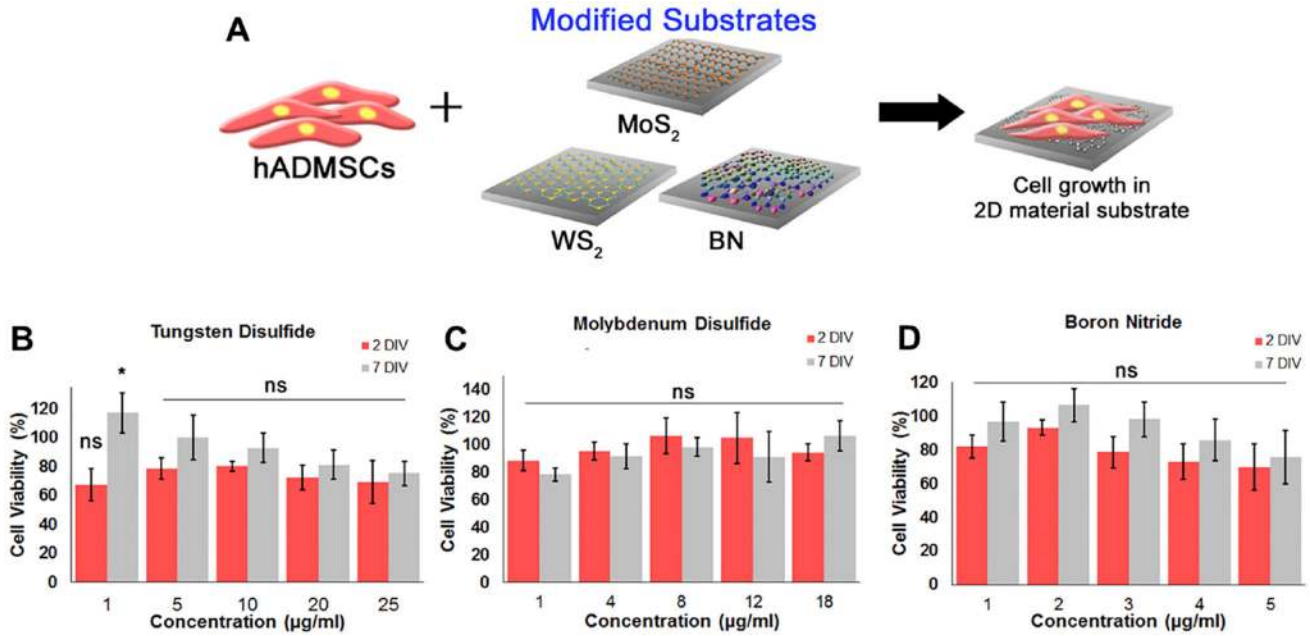

Figure 4.

Cytotoxicity of 2D material modified glass substrates. (A) Schematic of the experimental design. Human adiopose-derived mesenchymal stem cells (hADMSCs) were seeded onto glass substrates that were modified with a thin film of various 2D materials including molybdenum disulfide (MoS_2), tungsten disulfide (WS_2), and hexagonal boron nitride (BN). (B-D) Cell viability of the modified substrates after 2 days and 7 days as determined by growth rate using a CCK-8 assay. Figure adapted from reference[152]

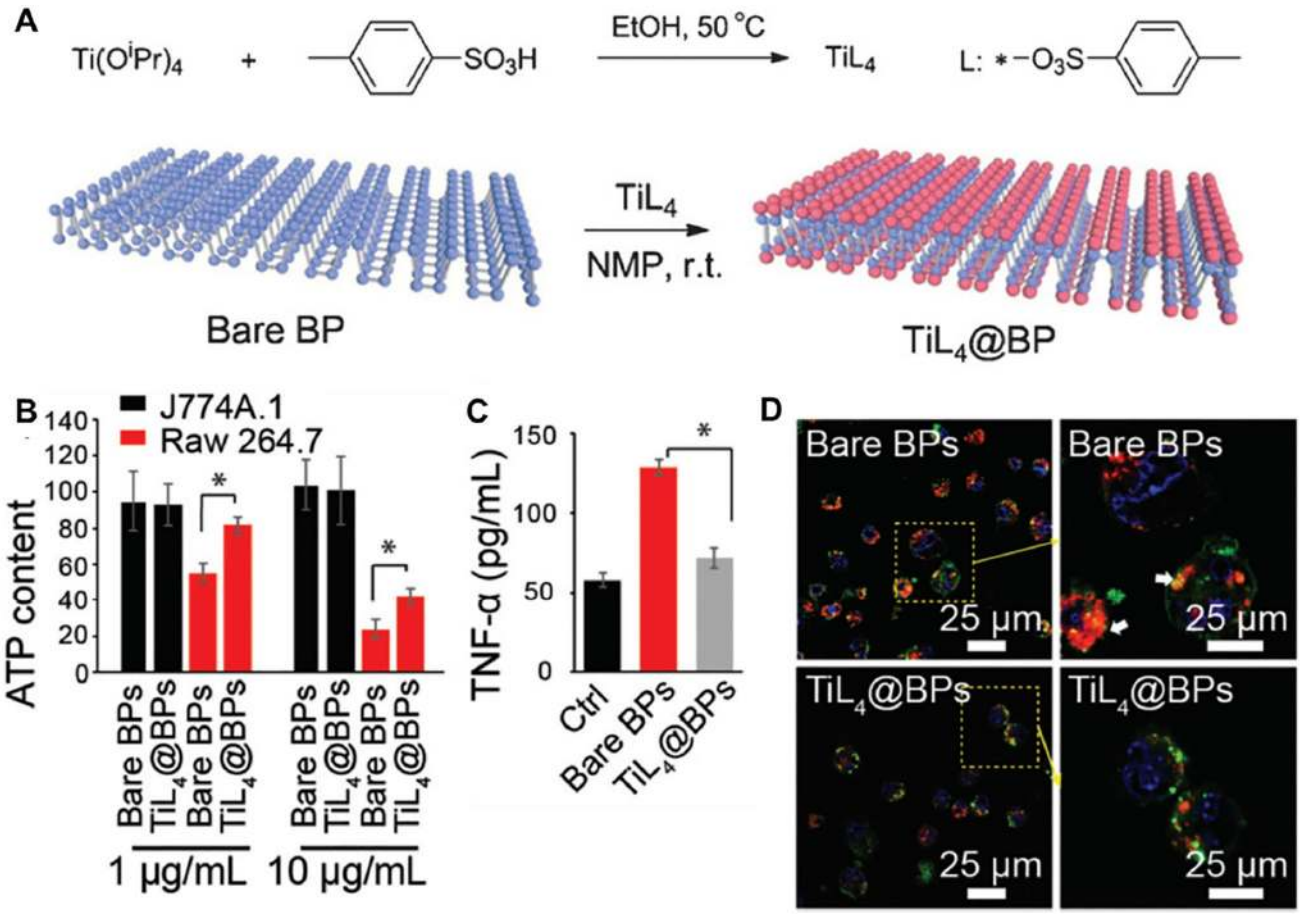

Figure 5.

Effects of chemical modification on the toxicity of black phosphorus (BP). (A) Synthesis scheme and illustration of the surface coordination of the titanium sulfonate ligand (TiL_4) to BP to generate TiL_4@BP. (B) Cell viability of raw 264.7 and J774A.1 cells after 24 hours exposure to bare BP and TiL_4@BP as determined by an ATP assay. (C) TNF-α production from raw 264.7 cells after 12 hours exposure to 10 μg mL^{-1} of the BP samples. (D) Confocal microscopy images of J774A.1 cells stained with Magic Red to show Cathepsin B location after exposure to the BP samples for 6 hours. In the control cells, cathepsin B appears as concentrated dots, localized within the lysosomes. After exposure to bare BP, the lysosomes appear swollen, while this inflammatory effect is not observed after exposure to TiL_4@BP. Figure adapted from reference[164]

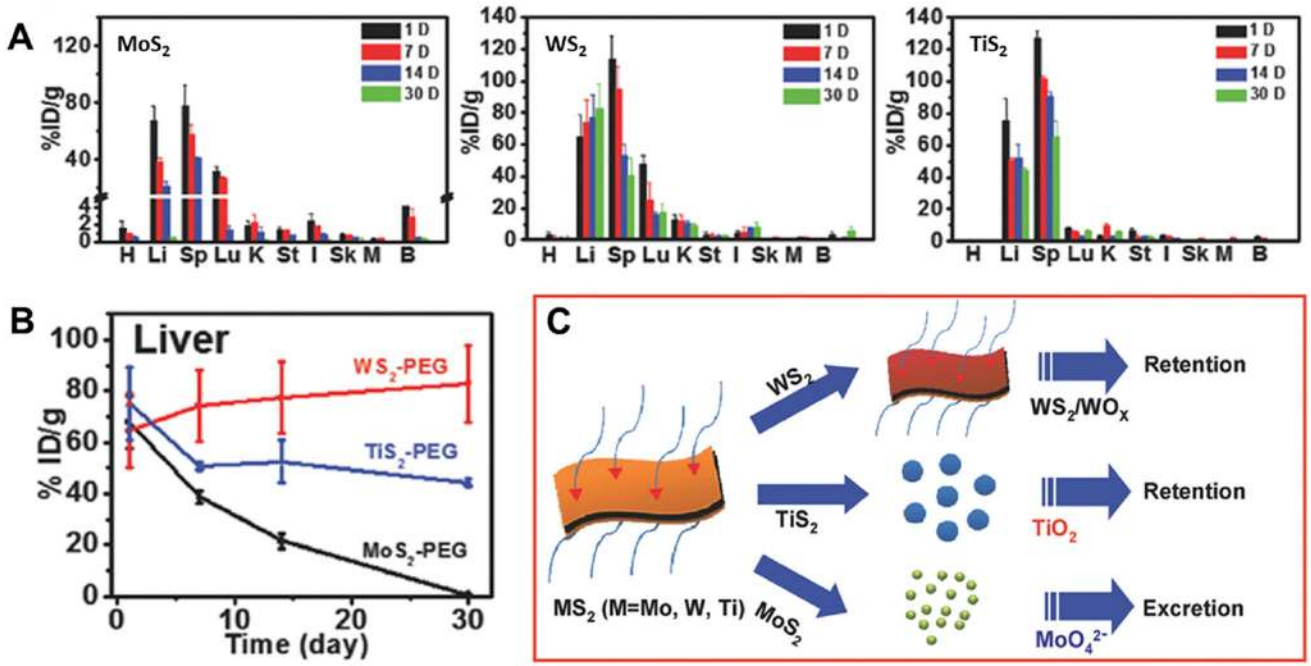

Figure 6.

Biodistribution and fate of PEGylated transition metal dichalcogenides (TMDCs). (A) *In vivo* biodistribution of PEGylated molybdenum disulfide (MoS_2), tungsten disulfide (WS_2), and titanium disulfide (TiS_2) in major organs of mice after intravenous injection for up to 30 days. All materials accumulated mainly in the liver and spleen, but after 30 days MoS_2 was cleared from the system while WS_2 and TiS_2 persisted. (B) Clearance of the PEGylated TMDCs from the liver over 30 days. (C) Schematic illustrating the chemical transformation of the PEGylated TMDCs. MoS_2 dissolves and forms soluble MoO_4^{2-}, which is excreted. TiS_2 oxidizes to form TiO_2, which is insoluble in aqueous solution and the aggregates are retained. WS_2 undergoes some oxidation, but its chemical stability leads to its retention in the organs. Figure adapted from reference[166]

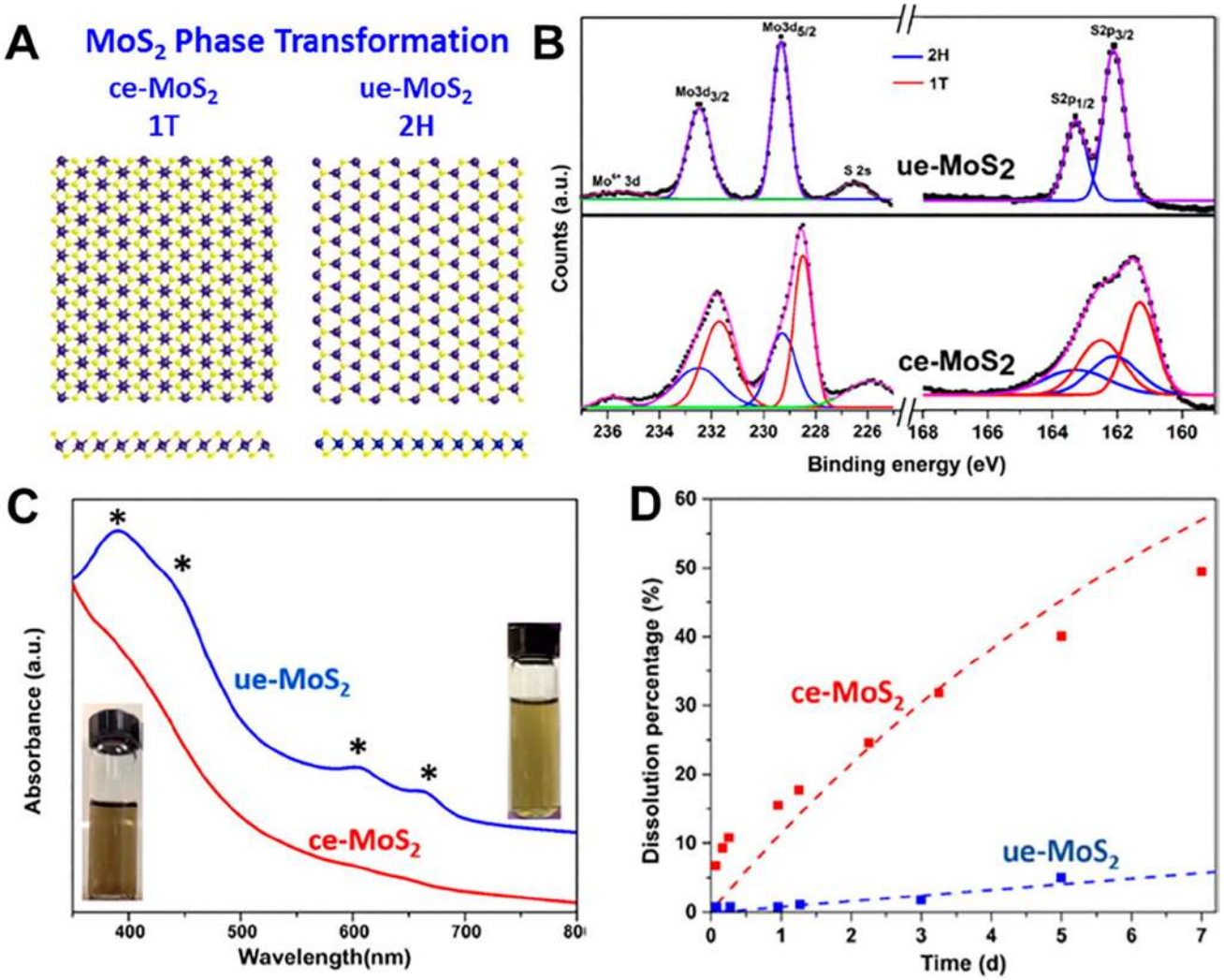

Figure 7.

Stability and dissolution of 1T and 2H phases of molybdenum disulfide (MoS_2). (A) Illustration of the 1T and 2H phases of MoS_2. Chemical exfoliation of MoS_2 (ce-MoS_2) results in a phase change to the 1T phase while ultrasonication-assisted exfoliation (ue-MoS_2) maintains the 2H phase. (B) XPS spectra and fitting of the Mo 3d and S 2p peaks of ce-MoS_2 and ue-MoS_2. ue-MoS_2 is in the 2H phase, while ce-MoS_2 contains both 1T and 2H phase materials. (C) UV-Vis spectra and pictures of ue-MoS_2 and ce-MoS_2. ue-MoS_2 shows the exciton peaks intrinsic to the 2H phase of the material. (D) Dissolution of ce-MoS_2 and ue-MoS_2 in HEPES buffer (pH 7), showing a significantly faster rate of dissolution for ce-MoS_2. Figure adapted from reference[171]

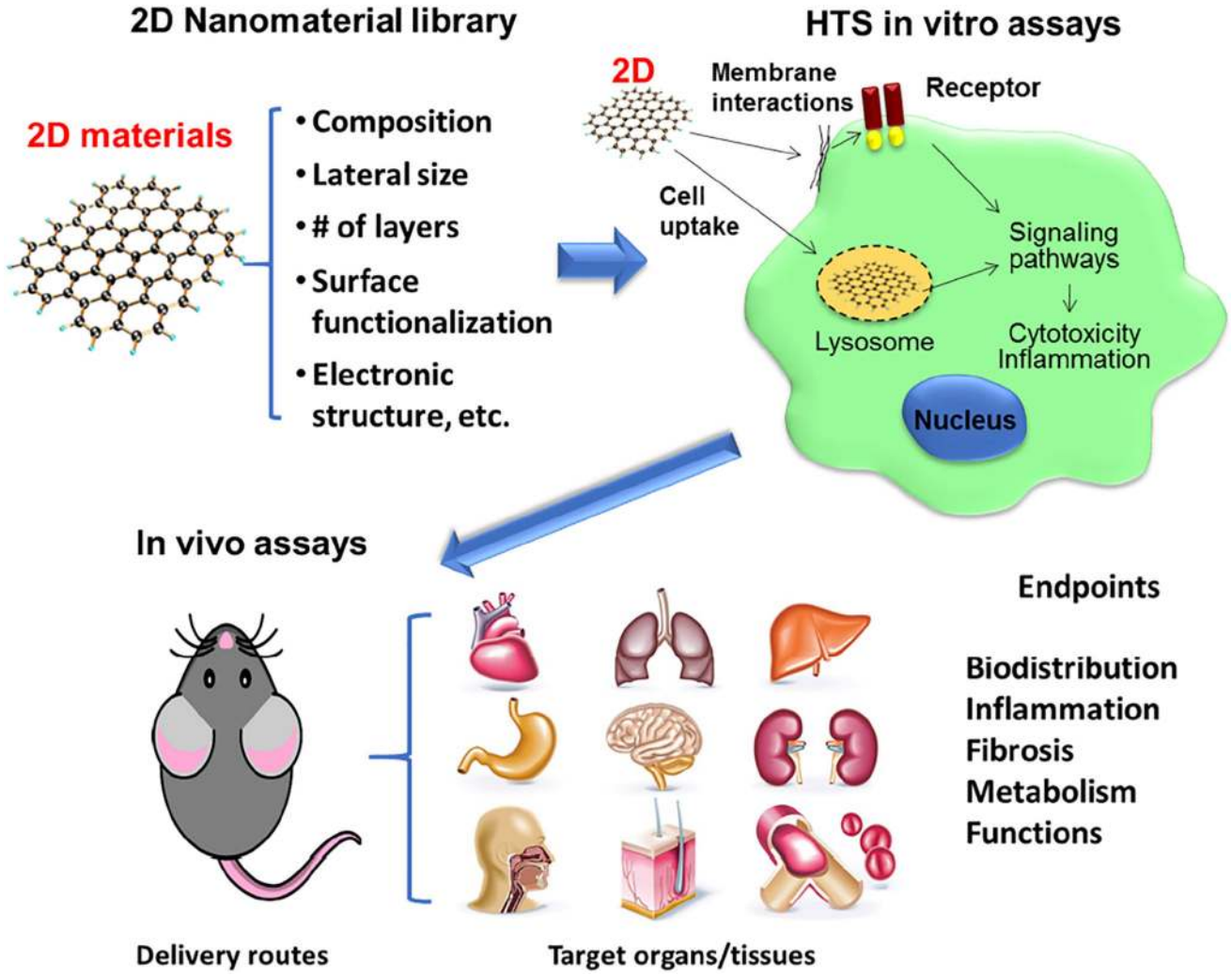

Figure 8.

A proposed approach for the hazard assessment of 2D materials. A library of 2D materials where the physicochemical properties are systematically varied and extensively characterized can be used to relate specific properties to biological outcomes. *In vitro* high throughput screening (HTS) assays can further be used to quantify a response for specific biological endpoints. From these assays, carefully selected *in vivo* assays can then be employed to validate the *in vitro* results and confirm the hazard potential of the 2D material.

Table 1.

Cytotoxicity evaluations of 2D materials. Reported cytotoxicity results for 2D materials are highly dependent on synthesis and preparation methods, material properties, and experimental parameters.

Composition (Phase)	Synthesis/Exfoliation	Size (Method)	Surface modification	Cytotoxicity cell system (Assay, time)	Cytotoxicity results	Additional toxicity assays	Ref
MoS_2 (1T)	Chemical exfoliation	Thickness: 5 nm (AFM) Lateral Size: 100 nm - 1 μm (SEM)	-	A549 (WST-8, 24 h)	≥80 % viability up to 200 μg/mL	-	125
MoS_2 (2H)	Bulk	Not exfoliated (Raman)	-	A549 (MTT and WST-8, 24 h)	64–82% cell viability between 200 and 400 μg/mL	-	189
MoS_2 (1T)	Chemical exfoliation (methyllithium)	Not exfoliated (Raman)	-	A549 (MTT and WST-8, 24 h)	64–82% cell viability between 200 and 400 μg/mL	-	129
MoS_2 (1T)	Chemical exfoliation (n-butyllithium)	Exfoliated (Raman)	-	A549 (MTT and WST-8, 24 h)	53–55% cell viability between 200 and 400 μg/mL	-	129
MoS_2 (1T)	Chemical exfoliation (tert-butyllithium)	Exfoliated (Raman)	-	A549 (MTT and WST-8, 24 h)	53–55% cell viability between 200 and 400 μg/mL	-	129
MoS_2 (2H)	Bulk	1–100 μm (SEM)	-	THP-1 and BEAS-2B (MTS, 24 h)	≥80 % viability up to 50 μg/mL	Cellular uptake, *in vitro* proinflammatory cytokine production, *in vivo* toxicity, acute and sub-chronic *in vivo* inflammatory effects	130
MoS_2 (1T)	Chemical exfoliation	Thickness: < 3 nm Lateral Size: 50 – 600 nm (AFM)	-	THP-1 and BEAS-2B (MTS, 24 h)	≥80 % viability up to 50 μg/mL	Cellular uptake, *in vitro* proinflammatory cytokine production, *in vivo* toxicity, acute and sub-chronic *in vivo* inflammatory effects	130
MoS_2 (2H)	Liquid phase exfoliation (aqueous)	Thickness: 3 – 10 nm Lateral Size: 10 – 150 nm (AFM)	Pluronic F87	THP-1 and BEAS-2B (MTS, 24 h)	≥80 % viability up to 50 μg/mL	Cellular uptake, *in vitro* proinflammatory cytokine production, *in vivo* toxicity, acute and sub-chronic *in vivo* inflammatory effects	130
MoS_2 (2H)	Liquid phase exfoliation (organic)	Thickness: 2–3 layers (TEM)	-	RAMEC and PC12 (SRB, 24 h)	≥90 % viability up to 50 μg/mL	Cell morphology and proliferation	131
MoS_2 (2H)	Mechanical exfoliation	Thickness: 3 – 4 layers (Raman) Lateral Size: 8 nm - 10 μm (SEM)	-	HEK293f (Calcein AM/ Ethidium homodimer-1, 4 – 48 h)	≥80 % viability up to 48 hr	Cell morphology, ROS, and mutagenicity assays	132

ACS Nano. Author manuscript; available in PMC 2018 September 10.

Composition (Phase)	Synthesis/Exfoliation	Size (Method)	Surface modification	Cytotoxicity cell system (Assay, time)	Cytotoxicity results	Additional toxicity assays	Ref
MoS_2 (2H)	Chemical vapor deposition	Thickness: 2 – 3 layers (Raman)	-	HEK293f (Calcein AM/ Ethidium homodimer-1, 4 – 48 h)	≥80 % viability up to 48 hr	Cell morphology, ROS, and mutagenicity assays	132
MoS_2	No details provided	441.2 nm (DLS)	-	HepG2 (WST-8, 24 h)	≥80 % viability up to 30 μg/mL	Cellular uptake, ROS, mitochondrial membrane potential, membrane damage, membrane transport, chemosensitive effects, and gene expression assays	134
MoS_2 (2H)	Liquid phase exfoliation (aqueous)	Lateral Size: 50 nm, 117 nm, 177 nm (TEM)	Sodium cholate	A549, AGS, THP-1 (Calcein AM/ Ethidium homodimer-1, 24 h)	No loss of viability up to 10 μg/mL (A529) < 50% viability at 10 μg/mL (AGS and THP-1)	Endotoxin detection, cytokine production, and dendritic cell activation	138
MoS_2 (2H)	Liquid phase exfoliation	Thickness: 1 – 8 monolayers Lateral Size: 100 – 400 nm (Supplier)	-	hADMSCs (WST-8, 2 – 7 d)	* Thin film No loss of viability up to 18 μg/mL	-	152
MoS_2 (2H)	Liquid phase exfoliation (aqueous)	Lateral Size: 50 – 350 nm (AFM)	1-pyrenesulfonic acid sodium salt	A549 and HaCaT (PI/ Annexin V staining, 24 h)	No loss of viability up to 100 μg/mL	-	153
MoS_2 (1T)	Chemical exfoliation	Lateral size: 50 – 500 nm (TEM)	-	HeLa, RAW 264.7 and hMDM (PI/ Annexin V staining, 24 h)	No loss of viability in any of the cell lines	Enzymatic degradation, cytotoxicity of degradation products, cellular interaction and uptake, and cytokine production	165
MoS_2 (1T)	Chemical exfoliation	Lateral size: 50 – 500 nm (TEM)	2-iodoacetamide	HeLa, RAW 264.7 and hMDM (PI/ Annexin V staining, 24 h)	No loss of viability in HeLa and hMDM cells ~20% loss of viability at 100 ^g/mL in RAW 264.7	Enzymatic degradation, cytotoxicity of degradation products, cellular interaction and uptake, and cytokine production	165
MoS_2	High temperature solution phase synthesis	91 nm (DLS)	lipoic acid conjugated 5 kDa PEG	RAW 264.7, 293T and 4T1 (MTT, 24 h)	≥70 % viability up to 200 μg/mL	*In vitro* cell membrane damage and ROS; *in vivo* biodistribution, clearance, and toxicology	166
MoS_2 (1T)	Chemical exfoliation	Thickness: ~1.2 nm Lateral Size: ~250 nm	-	TIB-67 and HTB-177 (WST-8, 24 – 72 h)	≥80 % viability up to 80 μg/mL	-	171

Composition (Phase)	Synthesis/Exfoliation	Size (Method)	Surface modification	Cytotoxicity cell system (Assay, time)	Cytotoxicity results	Additional toxicity assays	Ref
$NbTe_2$	Bulk	500–1000 nm (DLS)	-	A549 (WST-8, 24 h)	≥60 % viability up to 200 μg/mL	-	127
$TaTe_2$	Bulk	500–1000 nm (DLS)	-	A549 (WST-8, 24 h)	≥60 % viability up to 200 μg/mL	-	127
TiS_2	High temperature solution phase synthesis	102 nm (DLS)	lipoic acid conjugated 5 kDa PEG	RAW 264.7, 293T and 4T1 (MTT, 24 h)	≥70 % viability up to 200 μg/mL	*In vitro* cell membrane damage and ROS; *in vivo* biodistribution, clearance, and toxicology	166
VS_2	Chemical exfoliation	Lateral Size: 10 nm - 1 μm (SEM)	-	A549 (MTT and WST-8, 24 h)	43% viability at 50 μg/mL	-	126
VSe_2	Chemical exfoliation	Lateral Size: 10 nm - 1 μm (SEM)	-	A549 (MTT and WST-8, 24 h)	9% viability at 50 μg/mL	-	126
VTe_2	Chemical exfoliation	Lateral Size: 10 nm - 1 μm (SEM)	-	A549 (MTT and WST-8, 24 h)	8% viability at 50 μg/mL	-	126
VTe_2	Bulk	500–1000 nm (DLS)	-	A549 (WST-8, 24 h)	< 50% viability at 25 μg/mL < 10% viability at 200 μg/mL	-	127
WS_2 (2H)	Mechanical exfoliation	Thickness: 5 – 8 layers (Raman) Lateral Size: 8 nm - 10 μm (SEM)	-	HEK293f (Calcein AM/ Ethidium homodimer-1, 4 – 48 h)	≥80 % viability up to 48 hr	Cell morphology, ROS, and mutagenicity assays	132
WS_2 (2H)	Liquid phase exfoliation (aqueous)	Lateral Size: 50 – 350 nm (AFM)	1-pyrenesulfonic acid sodium salt	A549 and HaCaT (PI/ Annexin V staining, 24 h)	No loss of viability up to 100 μg/mL	-	153
WS_2	High temperature solution phase synthesis	72 nm (DLS)	lipoic acid conjugated 5 kDa PEG	RAW 264.7, 293T and 4T1 (MTT, 24 h)	≥70 % viability up to 200 μg/mL	*In vitro* cell membrane damage and ROS; *in vivo* biodistribution, clearance, and toxicology	166
WS_2 (1T)	Chemical exfoliation	Thickness: 20 nm (AFM) Lateral Size: 100 nm - 1 μm (SEM)	-	A549 (WST-8, 24 h)	≥80 % viability up to 400 μg/mL	-	125
WS_2 (2H)	Liquid phase exfoliation	Thickness: 1 – 4 monolayers Lateral Size: 50 – 150 nm (Supplier)	-	hADMSCs (WST-8, 2 – 7 d)	* Thin film No loss of viability up to 25 μg/mL	-	152

ACS Nano. Author manuscript; available in PMC 2018 September 10.

Composition (Phase)	Synthesis/Exfoliation	Size (Method)	Surface modification	Cytotoxicity cell system (Assay, time)	Cytotoxicity results	Additional toxicity assays	Ref
WSe_2 (1T)	Chemical exfoliation	Thickness: 7 nm (AFM) Lateral Size: 100 nm - 1 μm (SEM)	-	A549 (WST-8, 24 h)	< 50% viability at 100 μg/mL	-	125
hBN	Liquid phase exfoliation (aqueous)	Lateral Size: 50 – 350 nm (AFM)	1-pyrenesulfonic acid sodium salt	A549 and HaCaT (PI/ Annexin V staining, 24 h)	No loss of viability up to 100 μg/mL	-	153
hBN	Purchased	472.7 nm (DLS)	-	HepG2 (WST-8, 24 h)	≥80 % viability up to 30 μg/mL	Cellular uptake, ROS, mitochondrial membrane potential, membrane damage, membrane transport, chemosensitive effects, and gene expression assays	134
hBN	Liquid phase exfoliation	Thickness: 1 – 5 monolayers Lateral Size: 50 – 200 nm (Supplier)	-	hADMSCs (WST-8, 2 – 7 d)	* Thin film No loss of viability up to 5 μg/mL	-	152
BP	Bulk	> 20 μm (SEM)	-	A549 (WST-8 and MTT, 24 h	48% viability (WST-8) 34% viability (MTT) at 50 μg/mL	-	135
BP	Ground by hand in a mortar in NMP followed by ultrasonication	Thickness: 1.5 ± 0.8 nm Lateral Size: 2.7 ± 0.7 nm (AFM)	-	HeLa (Annexin V staining, 24 h)	36.6% viability at 200 μg/mL	*In vitro* ROS, DNA damage, *in vivo* toxicity, and biodistribution	136
BP	Liquid phase exfoliation (DMSO)	Thickness: 2 – 3 nm (S), 5.5 – 6.5 nm (M), 15 – 20 nm (L) Lateral Size: 4.5 0.6 nm (S), 118 ± 22 nm (M), 394 ± 75 nm (L) (AFM/SEM/TEM)	-	LO2 (WST-8, 12 – 48 h)	≥80 % viability up to 48 hr	Cell apoptosis and necrosis assay	139
BP	Liquid phase exfoliation (aqueous)	Thickness: 91.9 ± 32.0 nm (BP-1), 27.0 ± 12.0 nm (BP-2), 17.4 ± 9.1 nm (BP-3) Lateral Size: 884.0 ± 102.2 nm (BP-1), 425.5 ± 78.8 nm (BP-2), 208.5 ± 46.9 nm (BP-3) (AFM)	-	NIH 3T3, HCoEpiC, and 293T (RTCA, 12 – 48 h)	Size dependent toxicity for all cell lines: BP-1 > BP-2 > BP-3	Cell morphology, ROS, and cell membrane integrity	140
BP	Liquid phase exfoliation (NMP)	Thickness: 2.0 ± 0.6 nm Lateral size: 2.8 ± 1.5 nm	TiL_4	J774A.1 and RAW 264.7 (ATP, 24 h)	No loss in viability in J774A.1 < 30% viability for bare BP	*In vitro* inflammatory effects, cellular uptake, and *in vivo* inflammatory effects	164

ACS Nano. Author manuscript; available in PMC 2018 September 10.

Composition (Phase)	Synthesis/Exfoliation	Size (Method)	Surface modification	Cytotoxicity cell system (Assay, time)	Cytotoxicity results	Additional toxicity assays	Ref
					< 50% viability for TiL4@BP at 10 μg/mL in raw 264.7		